

# CrystEngComm

Accepted Manuscript



This is an *Accepted Manuscript*, which has been through the Royal Society of Chemistry peer review process and has been accepted for publication.

*Accepted Manuscripts* are published online shortly after acceptance, before technical editing, formatting and proof reading. Using this free service, authors can make their results available to the community, in citable form, before we publish the edited article. We will replace this *Accepted Manuscript* with the edited and formatted *Advance Article* as soon as it is available.

You can find more information about *Accepted Manuscripts* in the [Information for Authors](#).

Please note that technical editing may introduce minor changes to the text and/or graphics, which may alter content. The journal's standard [Terms & Conditions](#) and the [Ethical guidelines](#) still apply. In no event shall the Royal Society of Chemistry be held responsible for any errors or omissions in this *Accepted Manuscript* or any consequences arising from the use of any information it contains.

**$^{35}\text{Cl}$  Solid-State NMR Spectroscopy  
of HCl Pharmaceuticals and their Polymorphs  
in Bulk and Dosage Forms**

Andrew M. Namespetra, David A. Hirsh, Marcel P. Hildebrand,  
Anthony R. Sandre, Hiyam Hamaed, Jeremy M. Rawson  
and Robert W. Schurko<sup>†,\*</sup>

*<sup>†</sup> Department of Chemistry and Biochemistry, University of Windsor*

*Windsor, Ontario, Canada N9B 3P4*

\*Author to whom correspondence should be addressed.

E-mail: [rschurko@uwindsor.ca](mailto:rschurko@uwindsor.ca)

Tel: (519) 253-3000 x3548 - Fax: (519) 973-7098

Version 15 – June 24, 2016

## Abstract

Herein, we demonstrate the use of  $^{35}\text{Cl}$  solid-state NMR (SSNMR) at moderate (9.4 T) and high (21.1 T) magnetic field strengths for the structural fingerprinting of hydrochloride (HCl) salts of active pharmaceutical ingredients (APIs) and several polymorphs, in both bulk and dosage forms. These include salts of metformin, diphenhydramine, nicardipine, isoxsuprine and mexiletine (the crystal structure of a mexiletine polymorph is reported herein). Signal-enhancing pulse sequences utilizing frequency-swept pulses and broadband cross polarization were employed to significantly decrease experimental times. In most cases, powder X-ray diffraction (pXRD) patterns and  $^{13}\text{C}$  SSNMR spectra are not useful for characterizing the APIs in dosage forms, due to interfering signals from the excipients (e.g., fillers and binders). However, it is demonstrated that  $^{35}\text{Cl}$  SSNMR can be used independently to fingerprint individual APIs and to detect the nature of the solid phases in the dosage forms without interference from the excipient.  $^{35}\text{Cl}$  SSNMR experiments were also conducted on systems with multiple polymorphs (i.e., isoxsuprine HCl and mexiletine HCl), and the solid phases of these APIs in their dosage forms are identified.  $^{35}\text{Cl}$  EFG tensors obtained from plane-wave DFT calculations on model systems are also presented and discussed in the context of their relationship to the local hydrogen-bonding environments of the chloride ions. This methodology shows great promise for identification of solid phases and detection of polymorphs and impurities, which are matters of importance for quality assurance in the pharmaceutical industry.

## 1. Introduction

Most active pharmaceutical ingredients (APIs) are manufactured, distributed, and consumed as solids.<sup>1</sup> APIs exhibit structural variability in the solid state, leading to different physicochemical properties (e.g., stability, solubility, density, etc.), which can in turn affect their pharmacokinetic behaviour (e.g., absorption rate, bioavailability, etc.).<sup>2-4</sup> One such structural variation is polymorphism, in which the molecules can exist in more than one distinct structural arrangement.<sup>5</sup> Another is pseudopolymorphism, which refers to the formation of hydrates and solvates with distinct structures. It is crucial for the pharmaceutical industry to have techniques for the characterization and identification of polymorphs of APIs in their initial bulk forms and their final dosage formulations (e.g., tablets, capsules, etc.), since polymorphic variations in the dosage form may result in undesirable or unexpected properties.<sup>6</sup> Analytical techniques that can monitor changes to the structure of the API throughout the manufacturing process have potential to serve as quality assurance tools, especially when polymorphic transformations<sup>7</sup> are possible during tableting processes such as compression, heating, wet granulation and grinding.<sup>8,9</sup> Since excipients have been shown to modify API physicochemical properties (e.g., increased rate of degradation), API-excipient interactions must be accounted for.<sup>10</sup> As a result, there has been increasing interest in probing both API and excipient structures within their dosage formulations.<sup>11-14</sup>

Two conventional methods of polymorph differentiation are powder X-ray diffraction (PXRD) and <sup>13</sup>C solid-state NMR (SSNMR) spectroscopy; however, each method has its limitations with respect to studying dosage forms.<sup>15</sup> PXRD patterns are often uninformative for amorphous or partially amorphous API samples.<sup>16-18</sup> Furthermore, crystalline domains within the excipient can also produce XRD patterns that inhibit the identification of powder patterns

corresponding to the crystalline API (which is usually present in much less relative abundance).  $^{13}\text{C}$  SSNMR is routinely used as a structural probe of API polymorphs in crystalline and amorphous forms<sup>1, 13</sup> as well as the excipients in dosage forms.<sup>19</sup> However, the  $^{13}\text{C}$  SSNMR spectra of dosage forms are often ambiguous due to overlapping  $^{13}\text{C}$  resonances corresponding to both the excipient and the API (and of course, the peaks corresponding to carbon sites in the former are often much more intense, further complicating matters).

To address these concerns, a number of studies have been conducted that employ multinuclear SSNMR (e.g.,  $^2\text{H}$ ,  $^{14}\text{N}$ ,  $^{15}\text{N}$ ,  $^{17}\text{O}$ ,  $^{19}\text{F}$ ,  $^{23}\text{Na}$ ,  $^{31}\text{P}$ , etc.) as an alternative method for the structural analysis of APIs.<sup>11, 20-35</sup> Our research group and others have demonstrated that  $^{35}\text{Cl}$  SSNMR can function as a non-destructive structural probe and a technique for polymorph identification and screening of hydrochloride (HCl) APIs.<sup>36-39</sup> Given that more than 50% of APIs are produced as HCl salts,<sup>40</sup> the widespread use of  $^{35}\text{Cl}$  SSNMR in quality assurance, and research and development departments of pharmaceutical companies is promising.

Chlorine has two naturally occurring, NMR-active isotopes,  $^{35}\text{Cl}$  and  $^{37}\text{Cl}$ , which are both  $I = 3/2$  quadrupolar nuclei with relatively small quadrupole moments of  $-8.165$  and  $-6.435 \text{ fm}^2$ , respectively.<sup>41</sup> Due to its higher natural abundance (75.78%) and higher sensitivity (i.e., larger gyromagnetic ratio,  $\gamma(^{35}\text{Cl}) = 2.6242 \times 10^7 \text{ rad s}^{-1} \text{ T}^{-1}$ ),  $^{35}\text{Cl}$  is the preferred nucleus for SSNMR studies. However, the low Larmor frequency at moderate field strengths (e.g.,  $\nu_0(^{35}\text{Cl}) = 39.19 \text{ MHz}$  at 9.4 T) necessitates the use of specialized techniques to rapidly acquire  $^{35}\text{Cl}$  SSNMR spectra (*vide infra*). The acquisition, processing and spectral simulation of  $^{35}\text{Cl}$  central-transition (CT,  $m_I = +1/2 \leftrightarrow -1/2$ ) spectra allow for the determination of the  $^{35}\text{Cl}$  electric field gradient (EFG) tensor parameters (normally expressed as the quadrupolar coupling constant,  $C_Q$ , and the asymmetry parameter,  $\eta_Q$ , see **Table 1** for definitions), which describe the quadrupolar

interaction (QI). In some cases, it is also possible to determine the chemical shift (CS) tensor parameters, including the isotropic shift,  $\delta_{\text{iso}}$ , the span,  $\Omega$ , and the skew,  $\kappa$ , as well as the Euler angles  $\alpha$ ,  $\beta$  and  $\gamma$ , which describe the relative orientation of the EFG and CS tensors.<sup>42</sup> The chlorine EFG and CS tensors are very sensitive to subtle differences in the intricate hydrogen-bonding network involving the chloride anion, as demonstrated by Bryce and co-workers for HCl salts of amino acids.<sup>43-45</sup> As a result, the aforementioned parameters are unique for each distinct chlorine site, providing a distinct *spectral fingerprint* for each API and each of their respective polymorphs. Therefore, measurement of the  $^{35}\text{Cl}$  EFG and CS tensor parameters via  $^{35}\text{Cl}$  SSNMR, and comparison with theoretically derived tensors from plane-wave density functional theory (DFT), can lend insight into the number, lengths, spatial arrangements and nature of the hydrogen bonding interactions.

To date, studies of HCl APIs and their polymorphs using  $^{35}\text{Cl}$  SSNMR have focused on the APIs in their pure, bulk forms.<sup>36-39</sup> The application of  $^{35}\text{Cl}$  SSNMR for the differentiation of polymorphs of HCl APIs in dosage forms is advantageous because most excipients do not contain chlorine; thus, any signals present in the  $^{35}\text{Cl}$  SSNMR spectra are unique to the API. However, in dosage forms, the API often represents a small fraction of the total weight of the sample. The combination of an unreceptive nucleus and low concentrations of  $^{35}\text{Cl}$  nuclei can result in low signal-to-noise (S/N) ratios in the  $^{35}\text{Cl}$  NMR spectra, and correspondingly long experimental times.

To develop  $^{35}\text{Cl}$  SSNMR as an efficient and practical characterization technique for the pharmaceutical industry, experimental throughput must be increased. In particular, technologies or techniques must be applied that maximize S/N and spectral quality, whilst minimizing run times and associated expenses. Although  $^{35}\text{Cl}$  SSNMR spectra can be acquired with relative

rapidity at higher fields (e.g., 14.1 to 21.1 T), the availability and costs of such fields can be prohibitive. Therefore, it is also of interest to investigate the use of specialized pulse sequences for enhancement of S/N, which can be used for efficient acquisition of  $^{35}\text{Cl}$  SSNMR spectra at *both* moderate and high field strengths. In particular, the combined use of broadband excitation pulses (wideband uniform-rate smooth truncation, WURST pulses)<sup>46</sup> and Carr-Purcell Meiboom-Gill echo trains (i.e., the WURST-CPMG sequence),<sup>47,48</sup> and a new broadband cross-polarization routine known as broadband adiabatic inversion CP (BRAIN-CP),<sup>49</sup> play important roles in increasing experimental efficiency.

To this end, we present an investigation of the use of  $^{35}\text{Cl}$  SSNMR for the structural study of HCl APIs within both bulk and dosage forms, including the use of specialized pulse sequences for rapid spectral acquisition. PXRD and  $^{13}\text{C}$  SSNMR are used as supporting characterization techniques for both bulk and dosage forms. Three API systems are studied, including the HCl salts of metformin (**Metf**), diphenhydramine (**Diph**), and nicardipine (**Nica**) (**Scheme 1**). It is demonstrated that  $^{35}\text{Cl}$  SSNMR can be used to determine the nature of the solid phase of the API in both the bulk and dosage forms, via comparisons of the quadrupolar and CS parameters for each phase. In addition, two APIs with multiple polymorphs, HCl salts of mexiletine (**Mexi**) and isoxsuprine (**Isox**), are studied via  $^{35}\text{Cl}$  SSNMR to identify the phases present in their dosage forms. Finally, we briefly discuss the potential use for  $^{35}\text{Cl}$  SSNMR as a high-throughput screening technique for studying a variety of solid dosage forms, including micro- and nanosized API domains, as well as for quantification of APIs and structural prediction via NMR crystallography.

## 2. Experimental

**2.1 Materials.** Pharmaceutical-grade bulk samples of **Metf**, **Diph**, **Nica**, **Isox** and **Mexi** were purchased from Sigma-Aldrich Canada, Ltd. The samples had reported purities ranging between 98 and 99 wt-% and were used without further purification. **Metf** was stored at 4 °C as per directions on the label. The samples of the bulk APIs were prepared for NMR experiments by grinding with a mortar and pestle, followed by tight packing into their respective sample holders.

A 500 mg tablet of Rho-Metformin Fc and a 10 mg tablet of **Isox** were used as the dosage forms of **Metf** and **Isox**, respectively. For **Diph**, a 25 mg tablet of Benadryl<sup>®</sup> was used as the dosage form. All three of the tablets were prepared for experiments by crushing and grinding using a mortar and pestle. The dosage forms of **Nica** and **Mexi** were a 20 mg capsule manufactured by Mylan and a 200 mg capsule produced by Teva, respectively. These samples were prepared by separating the two halves of the casing, extracting the powder and grinding with a mortar and pestle. To quantitatively compare the amounts of APIs in the bulk and dosage forms, the weight percentages of chlorine in the bulk and dosage samples were calculated and tabulated in the Supporting Information (**SI**, **Tables S1** and **S2**, respectively). All of these dosage forms were obtained at local apothecaries.

**2.2 Polymorph Synthesis.** *Sample Preparation of Isox-II.* “**Isox-I**” refers to the polymorph of isoxsuprine HCl (**Isox**) obtained from Sigma-Aldrich without further processing and whose crystal structure was characterized by Yathirjan *et al.*<sup>50</sup> “**Isox-II**” is a polymorph of **Isox-I** and was prepared using commercial **Isox** via the method documented previously by our research group.<sup>37</sup>

*Sample Preparation of Mexi-II and Mexi-III.* “**Mexi-I**” is the name given to the polymorph of mexiletine HCl (**Mexi**) purchased from Sigma-Aldrich and characterized without further processing. Crystals of **Mexi-II**, another polymorph, were obtained by slow evaporation (i.e., over a period of approximately one week) of 30 mg (0.139 mmol) of **Mexi-I** from 0.25 mL of methanol. **Mexi-III**, a third polymorph, was prepared by heating approximately 1 g of **Mexi-I** in an oven for six hours at 160 °C, as described in a previous paper by our group.<sup>37</sup> The identities of all polymorphs were confirmed via PXRD (where crystal structures are available) and <sup>35</sup>Cl SSNMR (*vide infra*). The crystal structure for **Mexi-I** has been reported by Sivy *et al.*,<sup>51</sup> and we report the crystal structure of **Mexi-II** in the SI. The crystal structure of **Mexi-III** is unknown to date.

**2.3 <sup>35</sup>Cl SSNMR.** <sup>35</sup>Cl SSNMR at 9.4 T. <sup>35</sup>Cl SSNMR experiments were performed on a Varian Infinity Plus NMR spectrometer with an Oxford 9.4 T wide-bore magnet ( $\nu_0(^{35}\text{Cl}) = 39.26$  MHz and  $\nu_0(^1\text{H}) = 399.73$  MHz). A Varian/Chemagnetics 5 mm triple-resonance HXY MAS probe was used for all experiments. All samples were packed into shortened 5 mm outer diameter (o.d.) glass tubes, except for the **Metf** samples, which were packed in 5 mm o.d. zirconia MAS rotors. Chlorine chemical shifts were referenced to NaCl(s) ( $\delta_{\text{iso}} = 0.00$  ppm). Spectra were acquired using six different pulse sequences: Hahn-echo,<sup>52</sup> (Q)CPMG,<sup>53</sup> WURST-echo,<sup>54</sup> WURST-CPMG,<sup>47, 48</sup> BRAIN-CP/WURST-CPMG (BRAIN-CP/WCPMG)<sup>49</sup> and BRAIN-CP/echo.<sup>49</sup> The former four sequences are referred to as direct excitation (DE) methods and the latter two are broadband cross-polarization (BCP) techniques. Optimized acquisition parameters for these experiments are found in the SI (**Tables S3-S6**).

<sup>35</sup>Cl SSNMR at 21.1 T. High-field <sup>35</sup>Cl SSNMR experiments on **Metf**, **Diph** and **Nica** were performed on a Bruker Avance II spectrometer equipped with a 21.1 T ( $\nu_0(^{35}\text{Cl}) = 88.2$

MHz) standard-bore magnet at the National Ultrahigh-field NMR Facility for Solids in Ottawa, Ontario, Canada. Static experiments were conducted on samples packed in 4 mm o.d. glass tubes with a home-built 4 mm double-resonance HX probe, employing WURST-CPMG and Hahn-echo pulse sequences. The 21.1 T MAS NMR experiments were conducted using a 3.2 mm double-resonance HX MAS probe with Bloch decay, Hahn-echo, or DFS<sup>55,56</sup> pulse sequences at spinning speeds ( $\nu_{\text{rot}}$ ) of either 20 kHz or 22 kHz. High-field experiments for the bulk polymorphs and dosage forms of **Mexi** and **Isox** were conducted on an ultra-wide bore 900 MHz (21.1 T,  $\nu_0(^{35}\text{Cl}) = 88.13$  MHz) superconducting NMR magnet at the NHMFL in Tallahassee, Florida. Static experiments were performed using a 3.2 mm dual-channel MAS probe. Optimized acquisition parameters for all experiments conducted at 21.1 T are found in the **SI (Tables S7-S10)**.

The  $^{35}\text{Cl}$  SSNMR spectra from all experiments were processed using the NUTS software program from Acorn NMR. Analytical simulations of the processed spectra were generated using the WSolids software package.<sup>57</sup> The uncertainties in the EFG and CS tensor parameters were estimated by bidirectional variation of each parameter and visual comparison of the experimental and simulated spectra of the bulk compounds. The parameters from the NMR spectra of the dosage forms match those of the bulk forms within experimental uncertainty in each case.

**2.4  $^{13}\text{C}$  SSNMR.** All  $^{13}\text{C}$  SSNMR spectra were acquired using the variable-amplitude cross-polarization (VACP) technique with TPPM<sup>58</sup> decoupling under MAS conditions. Carbon chemical shifts were referenced to tetramethylsilane ( $\delta_{\text{iso}} = 0.00$  ppm), using the high-frequency shift of adamantane as a secondary reference ( $\delta_{\text{iso}} = 38.57$  ppm). All samples were packed into 4

mm o.d. zirconia rotors. For each sample, spectra were acquired at two different spinning speeds to identify spinning sidebands and isotropic centrebands.

*<sup>13</sup>C SSNMR at 9.4 T.* <sup>1</sup>H-<sup>13</sup>C VACP/MAS NMR spectra were acquired at 9.4 T on a Varian Infinity Plus NMR spectrometer ( $\nu_0(^{13}\text{C}) = 100.52$  MHz) for the bulk forms and tablets of **Metf**, **Diph**, as well as the polymorphs and dosage forms of **Mexi** and **Isox**. A Varian/Chemagnetics 4 mm double-resonance HX MAS probe was used for all experiments. Additional experimental details are listed in **Tables S11** and **S12**.

*<sup>13</sup>C SSNMR at 11.7 T.* <sup>1</sup>H-<sup>13</sup>C VACP/MAS NMR spectra of **Nica** was acquired using a Bruker Avance III spectrometer outfitted with an 11.7 T narrow bore magnet ( $\nu_0(^1\text{H}) = 498.14$  MHz,  $\nu_0(^{13}\text{C}) = 125.25$  MHz) and a 4 mm broadband double-resonance HX probe. Additional experimental details are listed in **Table S13**.

**2.5 Powder X-ray Diffraction.** PXRD patterns were obtained for all samples using a Bruker DISCOVER X-ray diffractometer equipped with an Oxford Cryosystems 700 Cryostream Plus Cooler and Cu-K $\alpha$  ( $\lambda = 1.54056$  Å) radiation source. A Bruker AXS HI-STAR area detector was run under General Area Diffraction Systems (GADDS) software. Each sample was mounted in a glass capillary tube and analyzed by two diffraction experiments with the detector set at  $2\theta$  angles of  $15^\circ$  and  $45^\circ$ , respectively. The resulting patterns were then co-added and compared to single crystal simulations that were prepared using either the PowderCell 2.4<sup>59</sup> or Mercury 3.1<sup>60, 61</sup> software packages.

**2.6 Plane-wave Density Functional Theory (DFT) Calculations.** Crystal structures of all APIs except for **Mexi-II** were obtained from the Cambridge Structural Database (CSD) using CCDC ConQuest Version 1.14 software.<sup>60, 62</sup> Geometry optimizations of all atomic positions were performed on the single crystal X-ray structures of **Metf**, **Diph**, **Nica** and **Mexi-II** (there is

not crystal structure for **Mexi-III**); calculations for other systems were reported in an earlier work.<sup>37</sup> Calculations of the <sup>35</sup>Cl EFG and nuclear shielding (NS) tensor parameters were performed on all model systems developed from known crystal structures. All calculations were conducted using the CASTEP<sup>63</sup> plane-wave density functional theory (DFT) code in the Materials Studio software package (version 5.0), applying the generalized gradient approximation (GGA) with revised Perdew, Burke and Ernzerhof (rPBE) functionals, on-the-fly pseudopotentials, a *k*-point spacing of 0.08 Å and a plane-wave basis set energy cut-off of 500 eV. The chlorine chemical shift values were determined with respect to NaCl(s) ( $\delta_{\text{iso}} = 0.0$  ppm), for which a nuclear shielding of 971.22 ppm was calculated. The calculations were carried out on the Shared Hierarchical Academic Research Computing Network (SHARCNET). Euler angles from these calculations were determined using the EFGShield software program.<sup>64</sup>

**2.7 Single Crystal X-ray Diffraction.** A single crystal of **Mexi-II** (colourless plate of dimensions 0.40 × 0.18 × 0.06 mm) was coated in paratone oil and mounted on a cryo-loop. X-ray data were collected at 150(2) K with graphite-monochromated Mo-K $\alpha$  radiation ( $\lambda = 0.71073$  Å) on a Bruker APEX-II X-ray diffractometer with a CCD area detector. The data were integrated using SAINT within the APEX-II software and an absorption correction was applied (multi-scan).<sup>65</sup> The structure was solved using direct methods and refinement carried out with full-matrix least squares on  $F^2$  within the SHELXTL software.<sup>66</sup> All non-H atoms were refined anisotropically. H atoms were added at calculated positions and refined using a riding model. Details of the crystallographic and refinement parameters are provided in **Table S14**, along with the crystallographic data in cif format. The structure has been deposited with the Cambridge Crystallographic Data Centre: deposition number 1478423.

### 3. Results and Discussion

Each API was analyzed using the following systematic procedure: First, the diffraction patterns acquired from PXRD experiments were compared to the simulated patterns derived from known single-crystal structures (where available) in order to confirm the identity of the solid crystalline phases. Second,  $^{35}\text{Cl}$  SSNMR experiments were performed on both bulk and dosage forms of the APIs to acquire high-quality  $^{35}\text{Cl}$  CT patterns, from which the EFG and CS tensor parameters could be determined via spectral simulations. Third,  $^{13}\text{C}$  SSNMR spectra were obtained for the bulk and dosage forms. Lastly, plane-wave DFT calculations were conducted on the geometry-optimized structures to obtain theoretical chlorine EFG and nuclear shielding (NS) tensor parameters and orientations (only for systems that have not been previously investigated). In the following sections, the data for each sample is discussed in the order outlined above (a summary of the DFT calculations is presented at the end). Most of the  $^{35}\text{Cl}$  SSNMR spectra that were acquired are presented in figures throughout this document; however, due to the large amount of data associated with each sample, only select PXRD patterns and  $^{13}\text{C}$  SSNMR spectra are shown (the remainder are located in the SI). To quantitatively compare the amounts of APIs in the bulk and dosage forms, their weight percentages of chlorine were calculated and tabulated in **Tables S1** and **S2**, respectively. Prior to making detailed comparisons of the individual bulk and dosage forms, it is useful to discuss some general observations for experiments and calculations on all of the APIs.

**3.1 General Observations. PXRD.** The collection of PXRD patterns is necessary for determining the identities of the solid phases for each of the “out-of-the-bottle” commercial bulk samples. This was accomplished by comparing experimental PXRD patterns to simulated patterns based on known crystal structures. In the case of the dosage forms, especially in cases

of low wt-% of API, there can be substantial interference between patterns arising from the excipient matrix and the solid phase(s) of the API (*vide infra*).

<sup>35</sup>Cl SSNMR. The main focus of this study is the acquisition of high quality <sup>35</sup>Cl SSNMR spectra of dosage forms to (i) establish lower detection limits and (ii) examine whether the API exists in a microcrystalline form, either in the same phase as the starting material, or in a new phase. <sup>35</sup>Cl SSNMR spectra acquired at 21.1 T have greater signal-to-noise (S/N) than those acquired at 9.4 T because of (i) the increased differences in Boltzmann populations at the higher field strengths and (ii) the fact that the breadths of the CT patterns, which are dominated by the second-order quadrupolar interaction (SOQI), scale inversely with increasing magnetic field, generally resulting in narrower patterns. Simulations of powder patterns from data at both fields allows for the refinement of the EFG and CS tensor parameters.<sup>67</sup> MAS NMR spectra acquired at high field strengths are useful for isolating values of  $\delta_{\text{iso}}$ ,  $C_Q$  and  $\eta_Q$  (anisotropic CS interactions are averaged by MAS). The MAS CT patterns at 9.4 T are too broad to allow for complete separation of spinning sidebands from the isotropic centreband for the samples discussed herein. We note that the acquisition of MAS spectra at very high field strengths is not absolutely necessary, but it does simplify the parameter choices for simulations of the static patterns in some cases. In addition, good estimates of Euler angles can usually be garnered both from symmetry arguments and DFT calculations (*vide infra*).

A variety of pulse sequences can be used for the acquisition of high-quality <sup>35</sup>Cl SSNMR spectra. The pulse sequences described herein are divided into two general categories: direct excitation (DE) and broadband cross polarization (BCP). Again, the DE sequences used in this work include Hahn echo,<sup>52</sup> (Q)CPMG,<sup>53</sup> double-frequency sweeps (DFS)-CPMG,<sup>55, 68-70</sup> WURST-echo<sup>54</sup> and WURST-CPMG.<sup>47, 48</sup> For <sup>1</sup>H-<sup>35</sup>Cl BCP SSNMR experiments, the BRAIN-

CP pulse sequence<sup>49</sup> was used in tandem with WURST-CPMG (for broadband refocusing). BRAIN-CP enables efficient cross polarization over a broad bandwidth, and is ideal for <sup>35</sup>Cl patterns of APIs, which typically range in breadth from ca. 50 to 250 kHz. In order to compare the efficiencies of the two classes of experiments, DE and BCP experiments were conducted on almost all of the samples using identical acquisition parameters and equal experimental times (see **Table S15** for details). Comparisons of DE and BCP spectra are not included for samples of **Diph** and **Mexi**, due to low CP efficiencies which largely arise from short  $T_{1\rho}(^1\text{H})$  values.

<sup>13</sup>C SSNMR. <sup>13</sup>C SSNMR is also used in this study as a fingerprinting technique to compare the API structures in the bulk and dosage forms. Peaks observed in the spectra of both bulk and dosage forms are identified as those belonging to the API, whereas peaks that are observed only in the spectra of the dosage form only are identified as excipient peaks. There are three spectral regions that are common to the <sup>13</sup>C NMR spectra of all dosage forms: 20 to 30 ppm, 60 to 75 ppm and 100 to 110 ppm. These regions are consistent with three common classes of excipients: polysaccharides, synthetic polymers and stearates, respectively. Since the latter two regions are broadened, it is possible that there exists a mixture of cellulose derivatives that serve as binding agents, such as hydroxypropyl methylcellulose (HPMC), hydroxyethyl cellulose (HEC) and hydroxypropyl cellulose (HPC), with a corresponding range of chemical shifts due to the variation in the numbers and types of alkyl side chains (**Scheme 2a**).<sup>19</sup> This characteristic region could also contain signal from starches, which are used as lubricants and tablet diluents,<sup>19</sup> or polyethylene glycol (PEG), a synthetic polymer that acts as an API carrier and stabilizer (**Scheme 2b**).<sup>71, 72</sup> Magnesium stearate (**Scheme 2c**), a lubricant that has been investigated using <sup>13</sup>C CP/MAS SSNMR,<sup>73</sup> registers a characteristic resonance at ca. 34 ppm, which is observed in the spectra of some dosage forms. The peak at 21 ppm suggests the presence

polyvinylpyrrolidone (PVP), a synthetic polymer used as a secondary binding agent (**Scheme 2d**).<sup>74</sup> It is important to note that when studying the dosage forms with <sup>13</sup>C SSNMR, excipient resonances can hinder the identification of the API structure (i.e., in cases where the much more intense peaks from the excipients and overlap with the less intense peaks of the API).

**3.2 Metformin HCl (Metf).** **Metf** is a biguanidine oral hypoglycemic agent that inhibits hepatic glucose release, and is prescribed to treat diabetes mellitus.<sup>75</sup> The crystal structure of **Metf** has previously been reported, and has a space group of  $P2_1/c$ .<sup>76</sup> The acquisition of PXRD patterns and subsequent comparison to the simulated powder patterns, generated from the known crystal structures, confirms the identity and crystallinity of the API in both dosage and tablet forms (**Figure S1**). The slight rounding of the baseline of the pattern of the dosage form can be attributed to the presence of amorphous excipient material.<sup>77</sup> In cases such as this, in which the dosage form contains a high weight percentage of API (i.e., API: 76 wt-%, Cl: 16% wt-%, **Table S1**), PXRD is good technique for comparing the crystal structures of the API in the bulk and dosage forms.

<sup>35</sup>Cl SSNMR. The <sup>35</sup>Cl static NMR spectra of both bulk and dosage samples of **Metf** acquired at 9.4 T each show a single CT pattern, corresponding to a single chlorine site (**Figure 1**). These patterns also have narrow breadths (ca. 33 kHz); hence, the effects of both the SOQI and CSA are clearly observable. Simulated spectra for both forms yield  $C_Q$  and  $\eta_Q$  values of 2.44(4) MHz and 0.61(5), respectively (all of the other parameters are summarized in **Table 1**).

Spectra of similar quality to those acquired at 21.1 T were acquired in comparable experimental times using the BRAIN-CP/echo pulse sequence at 9.4 T (**Figure 2**). For instance, the BRAIN-CP spectrum of bulk **Metf** has ca. eleven times the S/N of the corresponding DE spectrum (**Figure 2a, 2b**). Each spectrum was acquired in equal experimental times of 0.9 h;

however, the CP experiment has four times fewer scans, since its optimized recycle delay is four times longer than that of the DE experiment (i.e., since  $T_1(^{35}\text{Cl}) < T_1(^1\text{H})$ , see **Table S15** for detailed S/N measurements and parameters). The spectra of the dosage form, which were both acquired in 1.8 h periods, show a similar increase in the S/N of the BRAIN-CP spectrum (**Figure 2c, 2d**). The similarities in the CP efficiency for the bulk and dosage forms are consistent with the notion that the APIs exist as micro- or nano-crystalline dispersions, and that there are limited spin-spin interactions between nuclei of the API and the excipient matrix (i.e.,  $^{35}\text{Cl}$ - $^1\text{H}$  dipolar interactions are limited between the two phases because the excipient-API interface is small).

$^{13}\text{C}$  SSNMR. Peaks corresponding to the APIs are identified in the  $^1\text{H}$ - $^{13}\text{C}$  CP/MAS NMR spectra of both the bulk and tablet forms of **Metf** (see **Figure S2**). Since the peaks corresponding to the excipient do not overlap with those of the API, **Metf** represents an uncommon case in which  $^{13}\text{C}$  SSNMR is an adequate technique for the identification of the API within the dosage form. Further discussion is presented in the **SI**, including a full listing of carbon chemical shifts for both the API and species in the excipient matrix.

**3.3 Diphenhydramine HCl (Diph).** **Diph**, which is more commonly known by its brand name, Benadryl<sup>®</sup>, is an over-the-counter antihistamine. Bulk **Diph** crystallizes in the  $Pna2_1$  space group.<sup>78</sup> The PXRD pattern of the bulk form matches well with the simulated pattern from the crystal structure, confirming its identity. However, major differences between the pattern of the dosage form and simulation are observed (**Figure S3**). Broadening of the peaks between  $15^\circ$  and  $30^\circ$  are likely caused by the presence of microcrystalline cellulose (mcc).<sup>79, 80</sup> The absence and lowered intensity of API peaks in the tablet pattern could be ascribed to the low weight-percentage of API in the tablet (API: 6.1 wt-%, Cl: 0.74%). Since the

majority of the API peaks cannot be observed, PXRD is not a suitable technique for its identification in the dosage form.

<sup>35</sup>Cl SSNMR. <sup>35</sup>Cl SSNMR spectra of the bulk form of **Diph** acquired at both 9.4 and 21.1 T indicate a single Cl anion site, with analytical simulations revealing values of  $C_Q = 4.52(8)$  MHz and  $\eta_Q = 0.14(6)$  (**Figure 3, Table 1**). The corresponding spectra of the tablet form yield patterns that match those of the bulk form, confirming that the API has the same crystalline form in both materials. Unlike **Metf**, the weight percentage of chlorine in the tablet of **Diph** is very low, at 0.74 wt-%. Since the calculated mass ratio of chlorine in the bulk sample to the tablet is ca. 16:1, approximately 256 times the number of scans are necessary in the experiments on the dosage form to achieve similar S/N to that in the spectrum of the bulk sample (S/N increases by a factor of  $N^{1/2}$ , where  $N$  = number of scans); however, this extensive signal averaging is prohibitive in terms of overall experimental times. Hence, the static spectrum of the tablet at 9.4 T was acquired with only ca. 1.9 times the number of scans of the bulk experiment, and clearly has lower S/N than the spectrum of the bulk form. The low S/N of the spectrum is most evident in the central region, between the “horns” of the powder pattern, where the central discontinuity cannot be resolved; as such, there is significant uncertainty associated with the Euler angles. Due to poor CP efficiency, the <sup>1</sup>H-<sup>35</sup>Cl BRAIN-CP spectra of **Diph** are of low quality and are not included. Nonetheless, the DE spectra are of high enough quality to allow for the identification of the positions of the horns in the spectra, which in turn allow for accurate determination of the <sup>35</sup>Cl EFG parameters. At 21.1 T, the static spectrum of the tablet was acquired with ca. nine times the number of scans as the bulk sample, and has similar S/N; the CT powder pattern is well-resolved, allowing for the accurate determination of the EFG and CS tensor parameters.

$^{13}\text{C}$  SSNMR.  $^{13}\text{C}$  SSNMR spectra of **Diph** in both the dosage and tablet forms were acquired at 9.4 T (**Figure S4**). All peak assignments of the  $^{13}\text{C}$  SSNMR spectra are listed in **Table S17**. The aromatic carbons C(2), C(3) and C(4) are assigned to the region of the broadened, unresolved peak centered at 129 ppm. All API peaks were identified in the spectrum of the tablet with the exception of the C(5) resonance, which is masked by the broad patterns between ca. 50 and 90 ppm that arise from the excipients. These resonances are consistent with the presence of microcrystalline cellulose, and may be responsible for some of the peaks in the PXRD patterns. The  $^{13}\text{C}$  SSNMR spectrum of the dosage form does not reveal major changes to the carbon chemical shifts of the API, suggesting that the crystalline structure of **Diph** remains intact within the excipient (i.e., micro- or nanocrystalline phases). However, this is difficult to say with absolute certainty, since there are overlapping peaks from the API and excipient matrix.

In reviewing all of these data, it is clear that this sample represents a case where  $^{35}\text{Cl}$  SSNMR excels at polymorph identification in comparison to PXRD and  $^{13}\text{C}$  SSNMR experiments for two reasons: (i) the API constitutes a low wt-% of the dosage form, making reliable identification of crystalline phases via PXRD very difficult and (ii) the excipient matrix has  $^{13}\text{C}$  SSNMR resonances or patterns that obscure peaks from the API, hindering the use of  $^{13}\text{C}$  SSNMR to confirm the presence of certain solid phases of the API.

**3.4 Nicardipine HCl (Nica).** **Nica** is a calcium-channel inhibitor that is taken orally during hypertensive emergencies to reduce blood pressure.<sup>81</sup> The crystal structure of **Nica(β)**, which was reported by Moreno-Calvo *et al.*, has a space group of  $P\bar{1}$ .<sup>82</sup> The experimental PXRD pattern of the bulk form of **Nica** matches the simulated powder pattern of the known crystal structure for **Nica(β)** (**Figure S5**).<sup>82</sup> The well-resolved peaks and flat baseline are indicators of high crystallinity. In contrast, the powder pattern of the capsule has additional features that are

severely broadened, which indicate the presence of non-crystalline material (e.g., the amorphous phases within the excipient).<sup>77</sup> The peaks that can be resolved in the pattern of the capsule correspond to the most intense peaks in the pattern of the bulk form, which have diffraction angles of 8°, 14°, 15°, 18°, 20° and 23°. This points to another limitation of PXRD in the characterization of samples containing high concentrations of amorphous material: many of the peaks corresponding to the crystalline API are masked by the signal from the excipient. In such cases, it is unlikely that PXRD patterns can aid in differentiating structures arising from polymorphs, hydrates or solvates.

<sup>35</sup>Cl SSNMR. The <sup>35</sup>Cl static SSNMR spectrum of bulk **Nica** has reasonably good S/N and was acquired in ca. 0.7 hours at 9.4 T using the BRAIN-CP/WCPMG pulse sequence (**Figure 4**). In the spectrum of the dosage form, which took 13.9 h to acquire, the S/N is quite poor, due to the low weight percentage of chlorine (API: 12.3 wt-%, Cl: 0.84 wt-%). By contrast, static spectra acquired at 21.1 T for the bulk and dosage forms are both acquired very rapidly (40 and 42 min for the capsule and bulk samples, respectively). Spectral simulations of spectra of the bulk and dosage forms acquired at both fields clearly indicate that the form of the API in the dosage form matches that of **Nica(β)**.

To compare the efficiency of the acquisition of <sup>35</sup>Cl spectra of **Nica** using DE and BCP methods, BRAIN-CP/WCPMG and WURST-CPMG experiments were performed in equal amounts of time, using identical CPMG parameters (**Figure 5** for <sup>35</sup>Cl SSNMR spectra and **Tables S4 and S5** for experimental details). The number of scans was adjusted to account for the difference in the recycle delays of the DE and BCP experiments. For both bulk and dosage forms, the S/N ratios of the BRAIN-CP/WCPMG spectra are more than two times greater than those of the WURST-CPMG spectra (**Table S15**), indicating that there is efficient <sup>1</sup>H-<sup>35</sup>Cl

polarization transfer. This is in contrast to **Diph**, for which the CP was very inefficient (*vide supra*). CP is dependent upon (i) the  $^1\text{H}$ - $^{35}\text{Cl}$  dipolar coupling (which is dependent upon the inverse cube of the internuclear  $^1\text{H}$ - $^{35}\text{Cl}$  distances), and (ii) the longitudinal relaxation in the rotating frame,  $T_{1\rho}(^{35}\text{Cl})$  and  $T_{1\rho}(^1\text{H})$ . These relaxation time constants are dependent upon the  $^1\text{H}$ - $^{35}\text{Cl}$  dipolar coupling as well as the rates of local fluctuating magnetic fields created by a variety of motions. As a result, it is not straightforward to predict when CP will be efficient or not, based upon structure alone. Nonetheless, for systems such as **Nica**, and numerous other systems for which CP processes are efficient and signal enhancement of  $^{35}\text{Cl}$  SSNMR spectra is substantial,<sup>37</sup>  $^{35}\text{Cl}$  BCP SSNMR experiments are valuable as a rapid means of confirming the identities of polymorphs in dosage forms.

$^{13}\text{C}$  SSNMR. All resonances in the  $^{13}\text{C}$  SSNMR spectrum of the bulk **Nica** sample were easily assigned (**Figure S6** and **Table S18**). Once again, many of the  $^{13}\text{C}$  resonances of the API are obscured in the  $^{13}\text{C}$  SSNMR spectrum of the **Nica** dosage form, due to the low concentration of **Nica** in the capsule (12.3 wt-% API, **Table S2**). As before, of the resonances corresponding to the API that are visible, there are no apparent shift changes caused by interactions with the excipient.

Once again, it is demonstrated that “excipient noise” in both the PXRD pattern and  $^{13}\text{C}$  SSNMR spectrum of the dosage form interferes with API signal. However, the  $^{35}\text{Cl}$  SSNMR spectra of the **Nica** capsule are unaffected by the presence of excipients, which highlights its use as a selective probe for HCl APIs in dosage forms. In addition, there does not seem to be a significant difference in  $^1\text{H}$ - $^{35}\text{Cl}$  CP behaviour between the bulk and dosage forms, indicating that the API likely exists in micro- or nano-crystalline domains (this result is also consistent with the  $^1\text{H}$ - $^{13}\text{C}$  VACP/MAS NMR spectra discussed above).

**3.5 Application to systems with two or more known polymorphs.** In our recent study of HCl APIs,  $^{35}\text{Cl}$  SSNMR and DFT calculations were used to establish relationships between the hydrogen-bonding arrangement about the Cl anions and the  $^{35}\text{Cl}$  EFG parameters.<sup>37</sup> Herein, we describe the application of  $^{35}\text{Cl}$  SSNMR for the identification of the phase of the API contained within dosage forms of **Isox** and **Mexi**. However, unlike our previous work (in Hahn-echo experiments were used to study the bulk APIs), here, we have employed frequency-swept pulses and broadband CP methods to characterize APIs at 9.4 T. The reduced experimental times associated with these techniques make the study of dosage forms possible.

**3.5.1 Isoxsuprine HCl (Isox).** The crystal structures of the two documented polymorphs of the vasodilator, **Isox**, are reported by Yathirajan *et al.*<sup>50</sup> and Leger *et al.*,<sup>83</sup> which are designated as **Isox-I** and **Isox-II**, respectively. The PXRD pattern of the **Isox** tablet reveals clear interference from the excipient, as evidenced by the broadened region between diffraction angles of ca. 15 and 30° (**Figure 6**). Comparison of the PXRD patterns of the two bulk polymorphs and the tablet reveals that peaks at diffraction angles of 9°, 12°, 15°, 18°, and 27.5° and between 21° and 24° are shared by all three patterns. Since some peaks exist that are common to only **Isox-I** and the tablet, most notably at 17°, 26° and 35°, it is possible to make a tentative identification of **Isox-I** as the phase of the API in the tablet. Peaks unique to the tablet are observed in regions between ca. 19° and 20°, and from 21° to 24°, which may be attributed to microcrystalline cellulose excipients.<sup>80, 84</sup>

Analytical simulations of the  $^{35}\text{Cl}$  SSNMR spectra of the **Isox** tablet acquired at 9.4 T and 21.1 T reveal identical  $^{35}\text{Cl}$  EFG and CS parameters to those of **Isox-I** (**Figure 7** and **Table 3**), confirming that the API in the tablet has the **Isox-I** crystal structure. Again, the long experimental times needed for the experiments on the dosage sample result from the low-weight

percentage of Cl (API: 4.95%, Cl: 0.52 wt-%). The identical CP efficiencies observed in the BRAIN-CP experiments for the bulk and dosage forms confirm that the Cl sites are the same in each. The spectra of **Isox-I** and the dosage form acquired using BRAIN-CP/WCPMG have a S/N ratio approximately four times greater than the WURST-CPMG spectra acquired for the same length of time (**Figure 8** and **Table S15**). This is greater CP efficiency than is observed for **Isox-II**, for which an increase in S/N of 1.4 times is observed.

The  $^{13}\text{C}$  SSNMR spectra can be used to differentiate the two polymorphs of **Isox** in the bulk form by the unique chemical shifts in the fingerprinting regions of the spectra at ca. 155 ppm and in the aromatic region between ca. 110 and 135 ppm; all other chemical shift values are shared between the polymorphs (see **Figure 9**). However, due to the low weight percentage of API in the tablet (4.95 % by weight, see **Table S2**), the excipient signal is of very high intensity relative to that of the API. Despite optimization of the acquisition parameters (see **Figure S7**), long experimental times were required to obtain  $^{13}\text{C}$  signal from the API (e.g., 22.0 h, **Table S12**).

**3.5.2 Mexiletine HCl (Mexi).** **Mexi** is a local anaesthetic and antiarrhythmic agent.<sup>85</sup> Although the existence of six polymorphs has been reported (characterized via FT-IR, DSC, PXRD and SCXRD),<sup>51, 86, 87</sup> the only crystal structure that has been reported is that of **Mexi-I** (i.e., the polymorph studied by Sivy *et al.*).<sup>51</sup> In the current study, three polymorphs (**Mexi-I**, **Mexi-II** and **Mexi-III**) are investigated. It was previously demonstrated by our group that PXRD,  $^{35}\text{Cl}$  SSNMR and  $^{13}\text{C}$  SSNMR can distinguish the three bulk polymorphs of **Mexi**.<sup>37</sup> For this work, a single crystal of **Mexi-II** was successfully grown and its structure was determined by SCXRD (see **SI** for crystallographic data).

The PXRD pattern of the contents of the **Mexi** capsule bears strong resemblance to the pattern of the **Mexi-I** polymorph (**Figure 10**). The sharp peaks in the pattern are an indication of high crystallinity of the API, with very little interference from the excipient. Therefore, PXRD is an adequate technique for the identification of the phase of **Mexi** in its dosage form, largely because of the high wt-% of the API (API: 63.1%, Cl: 10.4%). Nevertheless, it is still of interest to see the value and efficiency of  $^{35}\text{Cl}$  SSNMR for the study of these samples.

The  $^{35}\text{Cl}$  SSNMR spectra of the bulk forms of **Mexi**, as well as the tablet form, are shown in **Figure 11**. There is enormous variation in the patterns. **Mexi-I** has a very broad spectrum arising from two overlapping patterns, whereas **Mexi-II** has a narrow CT pattern, which corresponds to a single Cl site. The spectrum of **Mexi-III** has a featureless peak ( $100 \pm 80$  ppm) which is narrow in comparison to typical second-order patterns, suggesting either disorder at the Cl site or perhaps a disproportionation product. A free-base form of **Mexi** has a known crystal structure,<sup>88</sup> however, simulated pXRD patterns based on this structure do not match those of **Mexi-III**. Thus, **Mexi-III** could be a distinct free base compound or another polymorph of an HCl salt; this will be the subject of a future investigation. The chlorine sites in **Mexi-I** and the capsule are equivalent based on the identical set of EFG and CS tensor parameters obtained via analytical simulations of the two spectra; therefore, the **Mexi-I** polymorph is of the same phase as the API contained in the dosage form. Since the CP efficiencies in experiments on the **Mexi** polymorphs are poor, only the spectrum of the capsule acquired using DE (i.e., WURST-echo pulse sequence) is shown.

Finally, the three polymorphs of **Mexi** in their bulk forms can be distinguished with  $^{13}\text{C}$  SSNMR by subtle differences in the spectra at four fingerprint regions where each polymorph displays a unique set of  $^{13}\text{C}$  chemical shifts: (i) between ca. 154 and 156 ppm, (ii) between ca. 70

and 72 ppm, (iii) between ca. 47 and 49 ppm, and (iv) between ca. 10 and 20 ppm (see **Figure 12**). However,  $^{13}\text{C}$  SSNMR is ineffective for the identification of the polymorph(s) contained in the dosage form of Mexi because all four of these regions are masked by excipient signal.

### 3.6 Plane-wave DFT calculations of $^{35}\text{Cl}$ EFG and NS tensors

The plane-wave DFT calculations yield not only the  $^{35}\text{Cl}$  EFG and NS tensor parameters for each system, but also the orientations of these tensors in the molecular frames (**Figure 13**), which are useful for obtaining sets of Euler angles describing the relative orientation of the EFG and NS tensors, as well as for understanding the relationships between the NMR tensor parameters and molecular structure. In this work, we focus our discussion upon the experimental and calculated  $^{35}\text{Cl}$  EFG tensors, as it has been observed in previous studies that they are significantly affected by the number of short  $\text{H}\cdots\text{Cl}$  contacts.<sup>36,37</sup> There are no similar simple trends for CS tensor parameters, though they are still useful for confirming spectral fingerprints.<sup>36,37</sup> Our discussion focuses on **Metf**, **Diph**, **Nica( $\beta$ )** and **Mexi-II (Isox and Mexi-I)** were discussed in our previous work). The agreement between experimental and calculated EFG tensor parameters is generally good (**Table 1**).

The presence of multiple  $\text{H}\cdots\text{Cl}$  contacts of less than 2.6 Å, the rough upper limit for  $\text{H}\cdots\text{Cl}$  hydrogen bonds,<sup>89</sup> can affect the chlorine EFG and CS tensor parameters and orientations; in particular, short  $\text{H}\cdots\text{Cl}$  contacts of 2.2 Å or less have the most influence on the  $^{35}\text{Cl}$  EFG tensors. For instance, in systems with a single short  $\text{H}\cdots\text{Cl}$  contact less than or equal to ca. 2.2 Å, the principal component of the EFG tensor with the largest absolute magnitude,  $V_{33}$ , is typically oriented near or along the direction of this short hydrogen bond.<sup>37</sup>

*Metf.* **Metf** has one distinct chlorine site with four  $\text{H}\cdots\text{Cl}$  contacts ranging from ca. 2.21 to 2.37 Å (**Table 2**). Our plane-wave DFT calculations predict that the sign of  $C_Q$  is negative

( $C_Q = -3.30$  MHz), and that the largest component of the  $^{35}\text{Cl}$  EFG tensor,  $V_{33}$ , is oriented near the shortest contact ( $r(\text{H}\cdots\text{Cl}) = 2.218$  Å,  $\angle(\text{H}-\text{Cl}-V_{33}) = 4.203^\circ$ , **Figure 13a**). The small absolute magnitude of  $C_Q$  is consistent with our previous structural categorizations for APIs, which predict similar quadrupolar parameters for Cl anions involved in four contacts with nitrogen-containing moieties, with no single short contact near 2.0 Å.<sup>37</sup> The  $^{35}\text{Cl}$  EFG tensor is predicted to be non-axially symmetric, as indicated by the moderate value of  $\eta_Q$ , indicating that there are additional, non-equivalent hydrogen-bonding interactions approximately perpendicular to the shortest H $\cdots$ Cl contact (i.e., the local ground-state electron density produces a non-axial EFG tensor). Indeed, there are two H $\cdots$ Cl contacts of comparable lengths, oriented near the directions of  $V_{11}$  and  $V_{22}$ .

*Diph.* The value of  $C_Q$  predicted by DFT calculations for **Diph** is significantly larger than the experimental value (**Table 1**). Since  $C_Q$  is heavily influenced by the lengths of the hydrogen bonds in single-contact systems, we suspect that the hydrogen atom positions obtained from the DFT geometry optimization may not be accurate (i.e., in particular, the shortest calculated H $\cdots$ Cl distance is shorter than the distance reported in the crystal structure,<sup>78</sup> resulting in an overestimation of the  $C_Q$  value). The single chlorine site in **Diph** is involved in one short H-bonding contact ( $r(\text{H}\cdots\text{Cl}) = 2.005$  Å). DFT calculations predict that  $V_{33}$  is oriented near this short contact ( $\angle(\text{H}-\text{Cl}-V_{33}) = 17.9^\circ$ , **Figure 13b** and **Table 2**). It has been shown for chlorine anions in HCl API systems that have only one H-bonding contact shorter than 2.2 Å, that the magnitude of  $C_Q$  generally increases as the contact distance shortens, and the sign of the calculated  $C_Q$  is negative.<sup>37</sup> Indeed, the calculated value of  $C_Q$  for the **Diph** Cl site is large and negative ( $C_Q = -6.28$  MHz), in agreement with these trends. Furthermore, the calculated value

of  $\eta_Q = 0.01$  indicates a  $^{35}\text{Cl}$  EFG tensor of near-axial symmetry with  $V_{33}$  as the distinct component, also consistent with previous observations.<sup>36, 37</sup>

*Nica*( $\beta$ ). The geometry-optimized structure of **Nica**( $\beta$ ) has one unique Cl site with a single short H $\cdots$ Cl contact at a length of 2.137 Å (**Table 2, Figure 13c**). The predicted  $C_Q$  of -6.18 MHz and  $\eta_Q$  of 0.60 are in very good agreement with the experimentally determined values of 5.97 MHz and 0.44, respectively. The  $V_{33}$  component lies approximately in the plane of  $V_{22}$  and  $V_{33}$  ( $V_{33}$  is oriented at 41.28° with respect to the direction of this contact). The unusual tensor orientation, along with the intermediate value of  $\eta_Q$ , suggests that the second-shortest H $\cdots$ Cl contact ( $r(\text{H}\cdots\text{Cl}) = 2.360$  Å (much longer than the H $\cdots$ Cl contacts of 2.2 Å or less which have the strongest influence on the EFG tensor) may be responsible for the non-axially symmetric EFG. This is in contrast to many of the one-contact systems discussed in our earlier work, which are most often associated with EFG tensors with higher axial symmetry (i.e.,  $\eta_Q$  is closer to 0).<sup>37</sup> Further structural optimization and investigation may help elucidate the reasons for these differences, but is beyond the scope of the current study.

*Mexi-II*. Finally, the plane-wave DFT geometry optimization of the atomic positions of **Mexi** reveal that there is a single chlorine site involved in three H $\cdots$ Cl contacts (see **Figure 13d**). DFT calculations predict a small, positive value of  $C_Q = 3.34$  MHz and a higher value of  $\eta_Q = 0.80$ , in reasonable agreement with experimental measurements (**Table 4**).  $V_{33}$  is not oriented near any of the directions of the short H $\cdots$ Cl contacts, which is in line with our previous predictions.<sup>37</sup>

In summary, the  $^{35}\text{Cl}$  EFG tensors predicted by plane-wave calculations all reveal relationships between tensor orientations and the local hydrogen bonding environments of the chlorine anions that are largely consistent with all previous observations by our group. The

theoretically predicted Euler angles aided in obtaining unique fits of the  $^{35}\text{Cl}$  static SSNMR spectra in some cases. These relationships may have great value in future structural prediction algorithms that may be useful for the discovery and characterization of unknown phases of solid APIs, including those in dosage forms. The values of  $C_Q$  obtained from our computations are most often larger in magnitude than their corresponding experimentally determined values; there is no systematic bias like this for any of the other parameters. As noted above, the magnitude of  $C_Q$  is strongly influenced by hydrogen atoms that are close to the chloride ions ( $\leq 2.2$  Å); unfortunately, accurate experimental data on hydrogen atom positions is not available for these systems, and predictions of these positions using plane-wave DFT calculations is not trivial.

#### 4. Conclusions and Future Outlook

It has been demonstrated that  $^{35}\text{Cl}$  SSNMR is a powerful tool for fingerprinting and characterizing the structure of HCl APIs in both bulk and dosage forms, due to the extreme sensitivity of  $^{35}\text{Cl}$  EFG tensors to subtle differences in molecular-level structures and hydrogen-bonding schema. It is possible to use  $^{35}\text{Cl}$  SSNMR to identify the phase of the API in the dosage form, as well as phase changes that may arise during the drug manufacturing process. In tandem with the plane-wave DFT calculations of  $^{35}\text{Cl}$  EFG tensors, spectral fitting is made easier, and it may be possible to discover new phases or impurity products that may arise during formulation production. The use of crystal structure prediction (CSP) NMR crystallography methods may be of particular value for determining structures from combinations of  $^1\text{H}$ ,  $^{13}\text{C}$ ,  $^{15}\text{N}$  and  $^{35}\text{Cl}$  SSNMR data,<sup>90,91</sup> even in dosage forms or amorphous phases.

$^{35}\text{Cl}$  SSNMR can serve as a complementary or stand-alone method for the characterization of HCl APIs. In cases where PXRD or  $^{13}\text{C}$  SSNMR are unsuitable for characterizing APIs in dosage forms (e.g., amorphous solids, excipient interference, lengthy

experimental times, etc.),  $^{35}\text{Cl}$  SSNMR can be used as a substitute. It is possible to acquire  $^{35}\text{Cl}$  SSNMR spectra of HCl pharmaceuticals in both bulk and dosage forms using moderate-field spectrometers (we have a current lower detection limit of ca. 0.5 wt-% Cl); hence, experiments at ultra-high fields are generally not required to accurately extract the  $^{35}\text{Cl}$  EFG tensor parameters. However, the application of experiments at higher fields (e.g., 14.1 T and upwards), along with the use of S/N-enhancing experiments like WURST-CPMG and BRAIN-CP, could permit high-throughput examinations of dosage forms, and improve the accuracy of the EFG and CS tensor parameters. Such experiments should be very valuable in assessing the solid phase of the API in multiple lots or batches of pills, which is important for quality and assurance. It is also clear that if APIs exist in nanodomains, that interactions between the API and the excipient could have a dramatic effect on the  $^{35}\text{Cl}$  EFG tensors and corresponding powder patterns; clearly, none of the samples herein have nanosized API domains, since the  $^{35}\text{Cl}$  SSNMR patterns are not indicative of distributions of quadrupolar and chemical shift parameters, nor do CP efficiencies dramatically differ between experiments on bulk and dosage forms; rather, they likely have microcrystalline domains of API (similar to the bulk phases) stabilized within the excipient.

Broadband CP (BCP) experiments have great value in three possible scenarios: (i) In many cases, the BCP spectra have considerably higher S/N than their DE counterparts, meaning that such experiments are desirable for obtaining high-quality spectra in an efficient manner. (ii) The BRAIN-CP experiment has variability in terms of CP efficiency akin to that observed in conventional CP/MAS NMR experiments; hence, there is much potential for the use of BCP methods for spectral editing. (iii) BCP methods may be used under conditions of dynamic nuclear polarization (DNP),<sup>92</sup> which could provide enormous signal gains, and permit the studies

of surfaces of micro- and nanocrystals of APIs.<sup>28</sup> Our research group is currently exploring all of these possibilities.

It is important to note that we have not yet attempted to quantify relative amounts of APIs from their <sup>35</sup>Cl SSNMR spectra; however, the best choice for this would be DE experiments. The only factors that determine the integrated intensities of powder patterns from unique Cl sites are the number of <sup>35</sup>Cl spins and the relaxation time constants,  $T_1(^{35}\text{Cl})$  and  $T_2^{\text{eff}}(^{35}\text{Cl})$ . If measurements of the relaxation time constants are made on pure bulk samples in advance, and identical <sup>35</sup>Cl excitation and <sup>1</sup>H decoupling fields are applied, then it is possible to obtain information on the relative amounts of HCl salts. Quantification of signals from BCP experiments would be more challenging, due to their dependence on the <sup>1</sup>H-<sup>35</sup>Cl dipolar coupling,  $T_{1\rho}(^{35}\text{Cl})$ , and cross relaxation, as discussed earlier; however, this may also be possible with carefully designed and parameterized experiments on sets of standards.

In examining each of the characterization methods and their application to the structural elucidation of HCl APIs, it is evident that <sup>35</sup>Cl SSNMR has significant advantages over PXRD and <sup>13</sup>C SSNMR for the identification of polymorphs in their dosage forms in certain cases, and can work equally well in tandem as a supporting spectroscopic technique. <sup>35</sup>Cl SSNMR is clearly a tool that should be added to the growing arsenal of characterization techniques used in the pharmaceutical industry, for purposes of identification, differentiation and discovery of new solid phases of APIs.

## 5. Acknowledgements

R.W.S. and J.M.R. thank the Natural Sciences and Engineering Research Council (NSERC, Canada) for Discovery Grants that permitted this research. R.W.S. is also grateful for an Early Researcher Award from the Ontario Ministry of Research and Innovation, a Discovery Accelerator Supplement from NSERC, and support from the University of Windsor in the form of a 50<sup>th</sup> anniversary Golden Jubilee professorship. A.M.N. and A.R.S. thank NSERC for Undergraduate Summer Research Assistantships (USRA). We are also grateful for the funding of the Laboratories for Solid-State Characterization at the University of Windsor from the Canadian Foundation for Innovation, the Ontario Innovation Trust, and the University of Windsor. This work was made possible, in part, by the facilities of the Shared Hierarchical Academic Research Computing Network (SHARCNET: [www.sharcnet.ca](http://www.sharcnet.ca)). We thank Dr. Kristopher J. Harris, Mr. Christopher O'Keefe and Dr. Victor Terskikh for acquiring <sup>35</sup>Cl SSNMR spectra at 21.1 T at the National Ultrahigh-Field NMR Facility for Solids (Ottawa, Canada), a national research facility funded by the Canada Foundation for Innovation, the Ontario Innovation Trust, Recherche Quebec, the National Research Council of Canada, and Bruker BioSpin (<http://www.nmr900.ca>). We also thank Stanislav Veinberg, Michael Jaroszewicz and Dr. Ivan Hung for acquiring <sup>35</sup>Cl SSNMR spectra at 21.1 T at the National High Magnetic Field Laboratory in Tallahassee, FL, and Dr. Valerie Seymour for conducting CASTEP calculations on several systems, as well as for making helpful comments on the manuscript.

## References

1. M. Geppi, G. Mollica, S. Borsacchi and C. A. Veracini, *Appl. Spectrosc. Rev.*, 2008, **43**, 202.
2. D. Hörter and J. B. Dressman, *Adv. Drug Del. Rev.*, 2001, **46**, 75.
3. J. Bauer, J. Morley, S. Spanton, F. J. J. Leusen, R. Henry, S. Hollis, W. Heitmann, A. Mannino, J. Quick and W. Dziki, *J. Pharm. Sci.*, 2006, **95**, 917.
4. S. R. Chemburkar, J. Bauer, K. Deming, H. Spiwek, K. Patel, J. Morris, R. Henry, S. Spanton, W. Dziki, W. Porter, J. Quick, P. Bauer, J. Donaubaue, B. A. Narayanan, M. Soldani, D. Riley and K. McFarland, *Organic Process Research & Development*, 2000, **4**, 413.
5. M. R. Caira, *Design of Organic Solids*, 1998, **198**, 163.
6. J. K. Haleblan and W. McCrone, *J. Pharm. Sci.*, 1969, **58**, 911.
7. D. Braga, F. Grepioni, L. Maini, K. Rubini, M. Polito, R. Brescello, L. Cotarca, M. T. Duarte, V. Andre and M. F. M. Piedade, *New J. Chem.*, 2008, **32**, 1788.
8. A. Bauer-Brandl, *Int. J. Pharm.*, 1996, **140**, 195.
9. H. K. Chan and E. Doelker, *Drug Dev. Ind. Pharm.*, 1985, **11**, 315.
10. B. Staniszk, K. Regulska, J. Kania and P. Garbacki, *Drug Dev. Ind. Pharm.*, 2013, **39**, 51.
11. K. M. N. Burgess, F. A. Perras, A. Lebrun, E. Messner-Henning, I. Korobkov and D. L. Bryce, *J. Pharm. Sci.*, 2012, **101**, 2930.
12. J. W. Lubach, B. E. Padden, S. L. Winslow, J. S. Salsbury, D. B. Masters, E. M. Topp and E. J. Munson, *Anal. Bioanal. Chem.*, 2004, **378**, 1504.
13. R. T. Berendt, D. M. Sperger, P. K. Isbester and E. J. Munson, *Trac-Trends Anal. Chem.*, 2006, **25**, 977.
14. T. Azaïs, C. Tourné-Péteilh, F. Aussenac, N. Baccile, C. Coelho, J.-M. Devoisselle and F. Babonneau, *Chem. Mater.*, 2006, **18**, 6382.
15. F. Vogt, *Am. Pharm. Rev.*, 2008, **11**, 50.
16. S. R. Byrn, R. R. Pfeiffer, G. Stephenson, D. J. W. Grant and W. B. Gleason, *Chem. Mater.*, 1994, **6**, 1148.
17. J. K. Haleblan, *J. Pharm. Sci.*, 1975, **64**, 1269.
18. B. Hancock and M. Parks, *Pharm. Res.*, 2000, **17**, 397.
19. D. M. Sperger and E. J. Munson, *AAPS PharmSciTech*, 2011, **12**, 821.
20. V. Chupin, A. I. P. M. De Kroon and B. De Kruijff, *J. Am. Chem. Soc.*, 2004, **126**, 13816.
21. J. M. Griffin, D. R. Martin and S. P. Brown, *Angew. Chem. Int. Ed.*, 2007, **46**, 8036.
22. Z. J. Li, Y. Abramov, J. Bordner, J. Leonard, A. Medek and A. V. Trask, *J. Am. Chem. Soc.*, 2006, **128**, 8199.
23. E. D. L. Smith, R. B. Hammond, M. J. Jones, K. J. Roberts, J. B. O. Mitchell, S. L. Price, R. K. Harris, D. C. Apperley, J. C. Cherryman and R. Docherty, *J. Phys. Chem. B*, 2001, **105**, 5818.
24. F. G. Vogt, J. Brum, L. M. Katrincic, A. Flach, J. M. Socha, R. M. Goodman and R. C. Haltiwanger, *Cryst. Growth. Des.*, 2006, **6**, 2333.
25. I. Wawer, M. Pisklak and Z. Chilmonczyk, *J. Pharm. Biomed. Anal.*, 2005, **38**, 865.
26. R. M. Wenslow, *Drug Dev. Ind. Pharm.*, 2002, **28**, 555.
27. F. G. Vogt, H. Yin, R. G. Forcino and L. Wu, *Mol. Pharm.*, 2013, **10**, 3433.
28. A. J. Rossini, C. M. Widdifield, A. Zagdoun, M. Lelli, M. Schwarzwälder, C. Copéret, A. Lesage and L. Emsley, *Journal of the American Chemical Society*, 2014, **136**, 2324.
29. F. G. Vogt, G. R. Williams, M. Strohmeier, M. N. Johnson and R. C. B. Copley, *J. Phys. Chem. B*, 2014, **118**, 10266.

30. N. M. Dicaire, F. A. Perras and D. L. Bryce, *Can. J. Chem.*, 2014, **92**, 9.
31. X. Kong, M. Shan, V. V. Tersikh, I. Hung, Z. Gan and G. Wu, *J. Phys. Chem. B*, 2013, **117**, 9643.
32. P. Przybylski, K. Pyta, K. Klich, W. Schilf and B. Kamieński, *Magn. Reson. Chem.*, 2014, **52**, 10.
33. K. Paradowska and I. Wawer, *J. Pharm. Biomed. Anal.*, 2014, **93**, 27.
34. H. G. Brittain, K. R. Morris, D. E. Bugay, A. B. Thakur and A. T. M. Serajuddin, *J. Pharm. Biomed. Anal.*, 1993, **11**, 1063.
35. F. G. Vogt, P. C. Dell'Orco, A. M. Diederich, Q. Su, J. L. Wood, G. E. Zuber, L. M. Katrincic, R. L. Mueller, D. J. Busby and C. W. DeBrosse, *J. Pharm. Biomed. Anal.*, 2006, **40**, 1080.
36. H. Hamaed, J. M. Pawlowski, B. F. T. Cooper, R. Q. Fu, S. H. Eichhorn and R. W. Schurko, *J. Am. Chem. Soc.*, 2008, **130**, 11056.
37. M. Hildebrand, H. Hamaed, A. M. Namespetra, J. M. Donohue, R. Fu, I. Hung, Z. Gan and R. W. Schurko, *CrystEngComm*, 2014, **16**, 7334.
38. F. G. Vogt, G. R. Williams, M. Strohmeier, M. N. Johnson and R. C. B. Copley, *J. Phys. Chem. B*, 2014, **118**, 10266.
39. M. K. Pandey, H. Kato, Y. Ishii and Y. Nishiyama, *Phys. Chem. Chem. Phys.*, 2016, **Online: 10.1039/C5CP06042G**.
40. L. D. B. Bighley, S. M.; Monkhouse, D. C., in *Encyclopedia of Pharmaceutical Technology*, ed. J. B. Swarbrick, J. C., Marcel Dekker, Editon edn., 1995, vol. 13, pp. 453.
41. P. Pyykko, *Mol. Phys.*, 2001, **99**, 1617.
42. J. L. Dye, A. S. Ellaboudy and J. Kim, *Solid State NMR of Quadrupolar Nuclei*, Marcel Dekker, Inc., New York, 1991.
43. D. L. Bryce and G. D. Sward, *J. Phys. Chem. B*, 2006, **110**, 26461.
44. D. L. Bryce, G. D. Sward and S. Adiga, *J. Am. Chem. Soc.*, 2006, **128**, 2121.
45. R. P. Chapman and D. L. Bryce, *Phys. Chem. Chem. Phys.*, 2009, **11**, 6987.
46. E. Kupce and R. Freeman, *J. Magn. Reson. A*, 1995, **115**, 273.
47. L. A. O'Dell and R. W. Schurko, *Chem. Phys. Lett.*, 2008, **464**, 97.
48. L. A. O'Dell, A. J. Rossini and R. W. Schurko, *Chem. Phys. Lett.*, 2009, **468**, 330.
49. K. J. Harris, A. Lupulescu, B. E. G. Lucier, L. Frydman and R. W. Schurko, *J. Magn. Reson.*, 2012, **224**, 38.
50. H. S. Yathirajan, B. Nagaraj, R. S. Narasegowda, P. Nagaraja and M. Bolte, *Acta Cryst. E*, 2004, **E60**, o2228.
51. J. Sivy, V. Kettmann and E. Fresova, *Acta Cryst. C.*, 1991, **C47**, 2695.
52. E. L. Hahn, *Physical Review*, 1950, **80**, 580.
53. F. H. Larsen, H. J. Jakobsen, P. D. Ellis and N. C. Nielsen, *J. Phys. Chem. A*, 1997, **101**, 8597.
54. R. Bhattacharyya and L. Frydman, *J. Chem. Phys.*, 2007, **127**.
55. D. Iuga, H. Schäfer, R. Verhagen and A. P. M. Kentgens, *J. Magn. Reson.*, 2000, **147**, 192.
56. R. W. Schurko, I. Hung and C. M. Widdifield, *Chem. Phys. Lett.*, 2003, **379**, 1.
57. K. Eichele and R. E. Wasylishen, *WSolids1: Solid-State NMR Spectrum Simulation*, version 1.17.30, University of Tübingen, Tübingen, Germany, 2001
58. A. E. Bennett, C. M. Rienstra, M. Auger, K. V. Lakshmi and R. G. Griffin, *J. Chem. Phys.*, 1995, **103**, 6951.
59. W. Kraus and G. Nolze, *PowderCell for Windows*, Berlin, Germany, 2000

60. I. J. Bruno, J. C. Cole, P. R. Edgington, M. Kessler, C. F. Macrae, P. McCabe, J. Pearson and R. Taylor, *Acta Crystallogr., Sect. B: Struct. Sci.*, 2002, **58**, 389.
61. C. F. Macrae, P. R. Edgington, P. McCabe, E. Pidcock, G. P. Shields, R. Taylor, M. Towler and J. van de Streek, *J. Appl. Crystallogr.*, 2006, **39**, 453.
62. F. H. Allen, *Acta Crystallogr., Sect. B: Struct. Sci.*, 2002, **58**, 380.
63. S. J. Clark, M. D. Segall, C. J. Pickard, P. J. Hasnip, M. J. Probert, K. Refson and M. C. Payne, *Z. Kristallogr.*, 2005, **220**, 567.
64. S. Adiga, D. Aebi and D. L. Bryce, *Can. J. Chem.*, 2007, **85**, 496.
65. Bruker APEX, v2. 1-0, Madison, WI, USA, 2007
66. G. M. Sheldrick, SHELXTL, v 6.14, Madison, WI, USA, 2005
67. W. P. Power, R. E. Wasylshen, S. Mooibroek, B. A. Pettitt and W. Danchura, *J. Phys. Chem.*, 1990, **94**, 591.
68. A. P. M. Kentgens and R. Verhagen, *Chem. Phys. Lett.*, 1999, **300**, 435.
69. H. Schäfer, Iuga, D., Verhagen, R., Kentgens, A.P.M. , *The Journal of Chemical Physics*, 2001, **114**, 3073.
70. H. Schäfer, D. Iuga, R. Verhagen and A. P. M. Kentgens, *J. Chem. Phys.*, 2001, **114**, 3073.
71. N. Yam, X. L. Li and B. R. Jasti, *Int. J. Pharm.*, 2011, **411**, 86.
72. V. M. Litvinov, S. Guns, P. Adriaensens, B. J. R. Scholtens, M. P. Quaedflieg, R. Carleer and G. Van den Mooter, *Mol. Pharm.*, 2012, **9**, 2924.
73. R. K. Harris, P. Hodgkinson, T. Larsson and A. Muruganantham, *J. Pharm. Biomed. Anal.*, 2005, **38**, 858.
74. T. J. Oh, J. H. Nam and Y. M. Jung, *Vib. Spectrosc.*, 2009, **51**, 15.
75. S. M. Setter, J. L. Iltz, J. Thams and R. K. Campbell, *Clin. Ther.*, 2003, **25**, 2991.
76. S. L. Childs, L. J. Chyall, J. T. Dunlap, D. A. Coates, B. C. Stahly and G. P. Stahly, *Cryst. Growth Des.*, 2004, **4**, 441.
77. A. R. West, *Solid State Chemistry and its Applications*, John Wiley & Sons, New York, 2005.
78. R. Glaser and K. Maartmann-Moe, *J. Chem. Soc.-Perkin Trans. 2*, 1990, 1205.
79. E. Roumeli, A. Tsiapranta, E. Pavlidou, G. Vourlias, K. Kachrimanis, D. Bikiaris and K. Chrissafis, *J. Therm. Anal. Calorim.*, 2013, **111**, 2109.
80. V. Kumar and S. H. Kothari, *Int. J. Pharm.*, 1999, **177**, 173.
81. H. D. E. Peacock W. F., Levy P. D., Rhoney D.H., Varon J., *Am. J. Emerg. Med.*, 2012, **30**, 981.
82. E. Moreno-Calvo, M. Munto, K. Wurst, N. Ventosa, N. Masciocchi and J. Veciana, *Mol. Pharm.*, 2011, **8**, 395.
83. J. M. Leger, A. Carpy and J. C. Colleter, *Acta Crystallogr. Sect. B-Struct. Commun.*, 1981, **37**, 1927.
84. E. Doelker, R. Gurny, J. Schurz, A. Jánosi and N. Matin, *Powder Technol.*, 1987, **52**, 207.
85. A. Dejgard, P. Petersen and J. Kastrup, *Lancet*, 1988, **1**, 9.
86. A. Kiss and J. Repasi, *Analyst*, 1993, **118**, 661.
87. M. Kuhnert-Brandstatter and R. Vollenklee, *Sci. Pharm.*, 1987, **55**, 13.
88. Z. A. Bredikhina, A. V. Kurenkov, D. B. Krivolapov and A. A. Bredikhin, *Tetrahedron-Asymmetry*, 2015, **26**, 577.
89. G. R. Desiraju; and T. Steiner, *The Weak Hydrogen Bond In Structural Chemistry and Biology*, Oxford University Press, Oxford and New York, 1999.

90. R. K. Harris, R. E. Wasylshen and M. J. Duer, eds., *NMR Crystallography*, John Wiley & Sons, Ltd., Chichester, U.K., 2009.
91. M. Baias, C. M. Widdifield, J.-N. Dumez, H. P. G. Thompson, T. G. Cooper, E. Salager, S. Bassil, R. S. Stein, A. Lesage, G. M. Day and L. Emsley, *PCCP*, 2013, **15**, 8069.
92. M. Rosay, L. Tometich, S. Pawsey, R. Bader, R. Schauwecker, M. Blank, P. M. Borchard, S. R. Cauffman, K. L. Felch, R. T. Weber, R. J. Temkin, R. G. Griffin and W. E. Maas, *PCCP*, 2010, **12**, 5850.

## Tables

**Table 1.** Experimental and calculated  $^{35}\text{Cl}$  EFG and CS tensor parameters for HCl APIs <sup>a</sup>

		$C_Q$ <sup>b</sup> (MHz)	$\eta_Q$ <sup>c</sup>	$\delta_{\text{iso}}$ (ppm) <sup>d</sup>	$\Omega$ (ppm) <sup>e</sup>	$\kappa$ <sup>f</sup>	$\alpha$ (°) <sup>g</sup>	$\beta$ (°)	$\gamma$ (°)
<b>Metf</b>	Exp.	2.44(4)	0.61(5)	60(2)	68(5)	0.82(10)	90(15)	6(4)	90(13)
	Calc.	-3.30	0.52	111	76	0.47	312	12	86
<b>Diph</b>	Exp.	4.52(8)	0.14(6)	51(7)	20(15)	0.48(15)	0(30)	0(9)	0(30)
	Calc.	-6.28	0.01	109	72	0.14	200	39	222
<b>Nica(β)</b>	Exp.	5.97(13)	0.44(11)	65(4)	75(35)	0.95(30)	0	0	0
	Calc.	-6.18	0.60	64	66	0.74	209	31	174

<sup>a</sup> The experimental uncertainty in the last digit(s) for each value is indicated in parentheses. <sup>b</sup>  $C_Q = eQV_{33}/h$ . <sup>c</sup>  $\eta_Q = (V_{11} - V_{22})/V_{33}$ . <sup>d</sup>  $\delta_{\text{iso}} = (\delta_{11} + \delta_{22} + \delta_{33})/3$ . <sup>e</sup>  $\Omega = \delta_{11} - \delta_{33}$ ; <sup>f</sup>  $\kappa = 3(\delta_{22} - \delta_{\text{iso}})/\Omega$ . <sup>g</sup> The Euler angles,  $\alpha$ ,  $\beta$  and  $\gamma$ , define the relative orientation of the CS and EFG tensors. The “ZYZ” convention for rotation is used herein, as described by Dye et al.<sup>42</sup> and as implemented in the WSolids<sup>57</sup> and EFGShield<sup>64</sup> software packages.

**Table 2.** Short H...Cl contacts and  $^{35}\text{Cl}$  EFG tensor parameters for HCl APIs <sup>a</sup>

Compound (and reference for crystal structures)	Space Group	Contact Type <sup>b</sup>	Contact Distance <sup>c</sup> (Å)	Angle between H-Cl contact and $V_{33}$ (°)	Exp. $C_Q$ (MHz)	Calc. $C_Q$ (MHz)	Exp. $\eta_Q$	Calc. $\eta_Q$
<b>Metf</b> <sup>76</sup>	$P2_1/c$	RNH <sub>2</sub> ...Cl	2.218	4.203	2.44(4)	-3.30	0.61(5)	0.52
		RNH <sub>2</sub> ...Cl	2.245	26.158				
		RNH <sub>2</sub> ...Cl	2.255	86.073				
		RNH <sub>2</sub> ...Cl	2.371	86.290				
<b>Diph</b> <sup>78</sup>	$Pna2_1$	R <sub>3</sub> NH <sup>+</sup> ...Cl	2.005	1.472	4.52(8)	-6.28	0.14(6)	0.01
<b>Nica(β)</b> <sup>82</sup>	$P\bar{1}$	R <sub>3</sub> NH <sup>+</sup> ...Cl	2.137	41.28	5.97(13)	-6.18	0.44(11)	0.60
		R <sub>3</sub> NH <sup>+</sup> ...Cl	2.360	99.49				

<sup>a</sup> Definitions of EFG and CS tensor parameters are given in **Table 1**. <sup>b</sup> Indicates the type of functional group involved in the H...Cl contacts. <sup>c</sup> The short H...Cl contacts (< 2.6 Å) as determined via geometry optimization with DFT plane wave calculations (see **Results and Discussion** for details).

**Table 3.** Experimental and calculated  $^{35}\text{Cl}$  EFG and CS tensor parameters for polymorphs of HCl APIs <sup>a</sup>

Compound		$C_Q$ (MHz)	$\eta_Q$	$\delta_{\text{iso}}$ (ppm)	$\Omega$ (ppm)	$\kappa$	$\alpha$ ( $^\circ$ )	$\beta$ ( $^\circ$ )	$\gamma$ ( $^\circ$ )
Isox-I	Exp.	5.50(15)	0.25(5)	120(10)	50(20)	0.50(40)	40(20)	55(15)	20(20)
	Calc.	6.75	0.17	104	52	0.32	50	50	173
Isox-II site 1	Exp.	6.4(1)	0.33(3)	130(10)	34(10)	0.0(5)	70(25)	70(25)	0(25)
	Calc.	8.60	0.34	112	46	0.62	285	65	166
Isox-II site 2	Exp.	5.7(1)	0.31(3)	125(5)	47(20)	-0.4(5)	0(25)	0(25)	0(25)
	Calc.	7.02	0.31	102	46	0.51	282	52	205
Mexi-I site 1	Exp.	5.45(10)	0.40(8)	90(5)	80(20)	-0.80(20)	40(30)	100(20)	0
	Calc.	7.23	0.29	77	109	-0.81	26	78	10
Mexi-I site 2	Exp.	3.10(10)	0.55(10)	130(5)	75(20)	0.80(20)	10(10)	5(5)	0
	Calc.	3.03	0.86	102	74	0.75	264	88	131
Mexi-II	Exp.	1.99(10)	0.62(3)	55(4)	30(3)	-0.30(10)	92(5)	45(3)	50(10)
	Calc.	3.34	0.80	97	97	-0.06	30	85	24
Mexi-III <sup>b, c</sup>	Exp.	----	----	100(80)	----	----	----	----	----
	Calc.	----	----	----	----	----	----	----	----

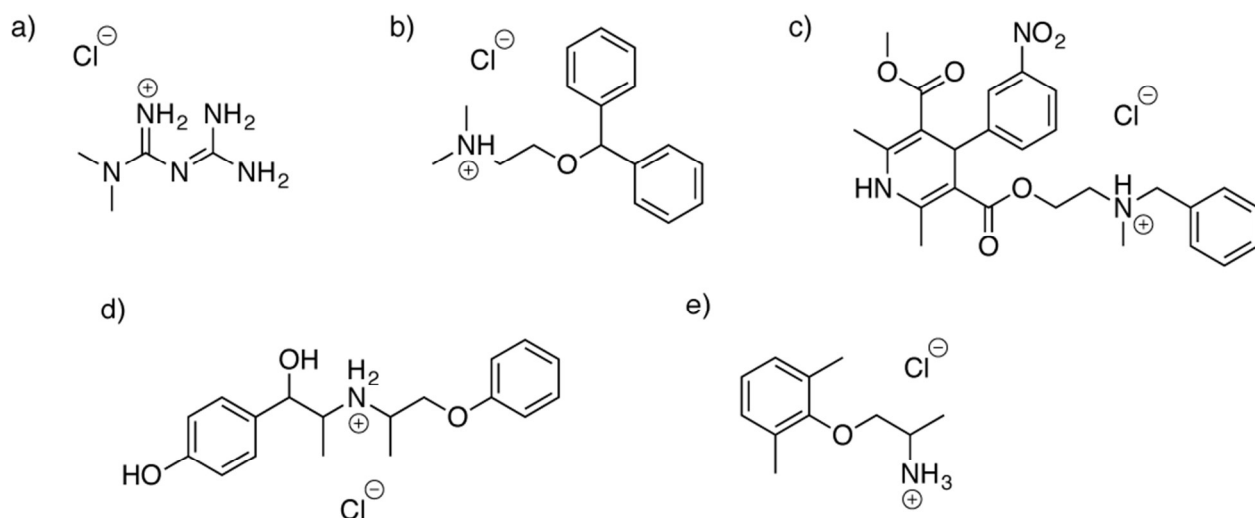
<sup>a</sup> Definitions of EFG and CS tensor parameters are given in **Table 1**. A full  $^{35}\text{Cl}$  SSNMR study of **Isox**, **Mexi** and their polymorphs, is presented elsewhere.<sup>37</sup> <sup>b</sup> No crystal structure is available. <sup>c</sup> Accurate determination of the  $^{35}\text{Cl}$  NMR parameters via analytical simulation is not possible due to the broad and featureless  $^{35}\text{Cl}$  powder pattern.

**Table 4.** Short H...Cl contacts and  $^{35}\text{Cl}$  EFG tensor parameters for HCl pharmaceutical polymorphs <sup>a</sup>

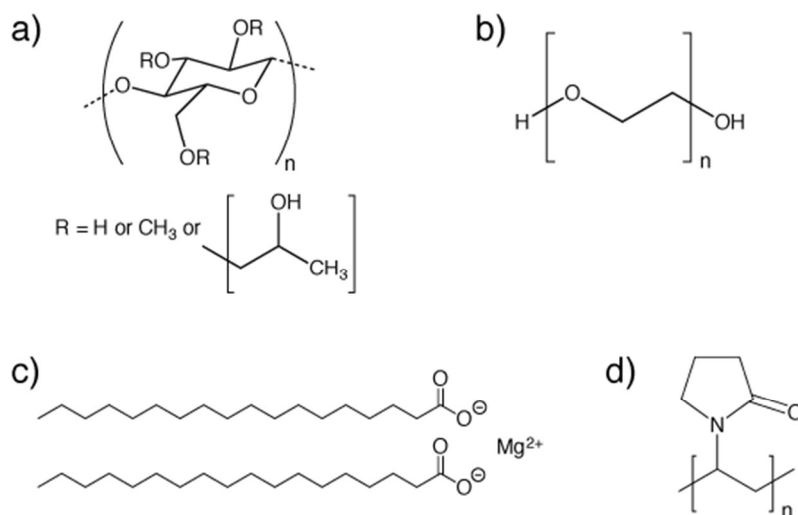
Compound	Space Group	Contact Type <sup>b</sup>	Contact distance (Å) <sup>c</sup>	Angle between H...Cl contact and $V_{33}$ (°)	Exp. $C_Q$ (MHz)	Calc. $C_Q$ (MHz)	Exp. $\eta_Q$	Calc. $\eta_Q$
Isox-I	$P2_1/c$	ROH...Cl	2.137	39.377	5.50(15)	6.75	0.25(5)	0.17
		R <sub>2</sub> NH <sub>2</sub> <sup>+</sup> ...Cl	2.139	78.429				
		ROH...Cl	2.168	87.862				
		R <sub>2</sub> NH <sub>2</sub> <sup>+</sup> ...Cl	2.383	69.996				
Isox-II site 1	$P\bar{1}$	R <sub>2</sub> NH <sub>2</sub> <sup>+</sup> ...Cl	2.087	84.582	6.4(1)	8.60	0.33(3)	0.34
		ROH...Cl	2.153	67.246				
		ROH...Cl	2.182	79.911				
		R <sub>2</sub> NH <sub>2</sub> <sup>+</sup> ...Cl	2.255	80.574				
Isox-II site 2	$P\bar{1}$	R <sub>2</sub> NH <sub>2</sub> <sup>+</sup> ...Cl	2.117	73.784	5.7(1)	7.02	0.31(3)	0.31
		ROH...Cl	2.121	56.270				
		ROH...Cl	2.191	87.183				
		R <sub>2</sub> NH <sub>2</sub> <sup>+</sup> ...Cl	2.420	81.650				
Mexi-I site 1	$P\bar{1}$	RNH <sub>3</sub> <sup>+</sup> ...Cl	1.996	71.397	5.45(10)	7.23	0.40(8)	0.29
		RNH <sub>3</sub> <sup>+</sup> ...Cl	2.058	82.755				
Mexi-I site 2	$P\bar{1}$	RNH <sub>3</sub> <sup>+</sup> ...Cl	2.123	89.700	3.10(10)	3.03	0.55(10)	0.86
		RNH <sub>3</sub> <sup>+</sup> ...Cl	2.138	77.641				
		RNH <sub>3</sub> <sup>+</sup> ...Cl	2.318	63.422				
		RNH <sub>3</sub> <sup>+</sup> ...Cl	2.342	36.707				
Mexi-II	$Pbcn$	RNH <sub>3</sub> <sup>+</sup> ...Cl	2.123	33.085	1.99(10)	3.34	0.62(3)	0.80
		RNH <sub>3</sub> <sup>+</sup> ...Cl	2.125	54.090				
		RNH <sub>3</sub> <sup>+</sup> ...Cl	2.158	54.939				
Mexi-III <sup>d,e</sup>	----	----	----		----		----	

<sup>a</sup> Definitions of EFG and CS tensor parameters are given in **Table 1**. <sup>b</sup> Indicates the functional group contributing to the H...Cl short contacts. <sup>c</sup> The shortest H...Cl contacts (< 2.6 Å) as determined via energy minimization and geometry optimization with DFT plane wave calculations (see the **Experimental** section for details). <sup>d</sup> No crystal structure available. <sup>e</sup> Accurate determination of the  $^{35}\text{Cl}$  NMR parameters via analytical simulation is not possible due to the featureless  $^{35}\text{Cl}$  powder pattern.

## Figures



**Scheme 1.** Schematic representations of (a) metformin HCl (**Metf**), (b) diphenhydramine HCl (**Diph**), (c) nicardipine HCl (**Nica**), (d) isoxsuprine HCl (**Isox**), and (e) mexiletine HCl (**Mexi**).



**Scheme 2.** Schematic representations of excipients: (a) hydroxypropyl methyl cellulose (HPMC), (b) polyethylene glycol (PEG), (c) magnesium stearate, (d) polyvinylpyrrolidone (PVP).

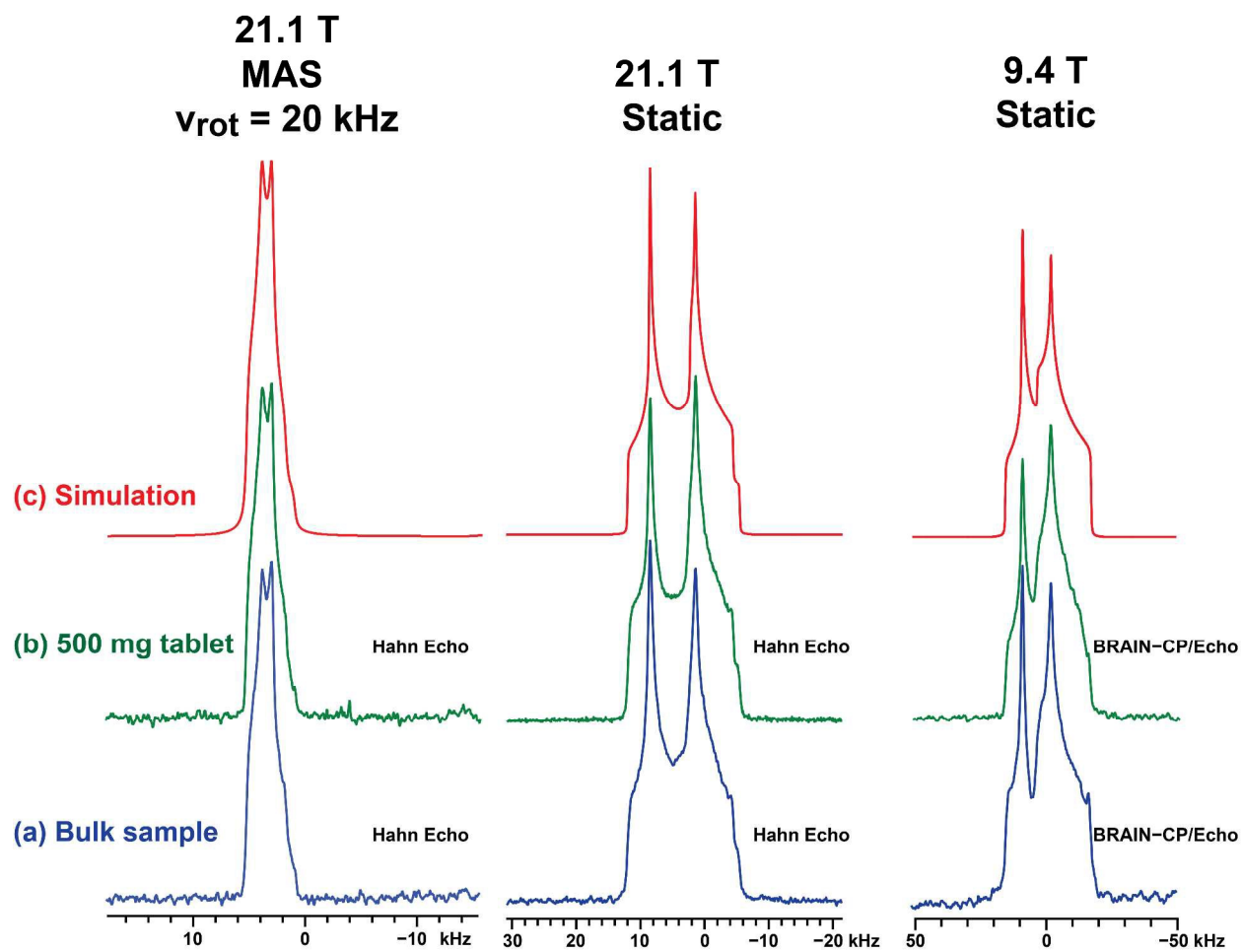


**Figure 1.**  $^{35}\text{Cl}$  SSNMR spectra of the (a) bulk **Metf** sample, (b) **Metf** dosage form, and (c) analytical simulations. All acquisition parameters are given in the SI.

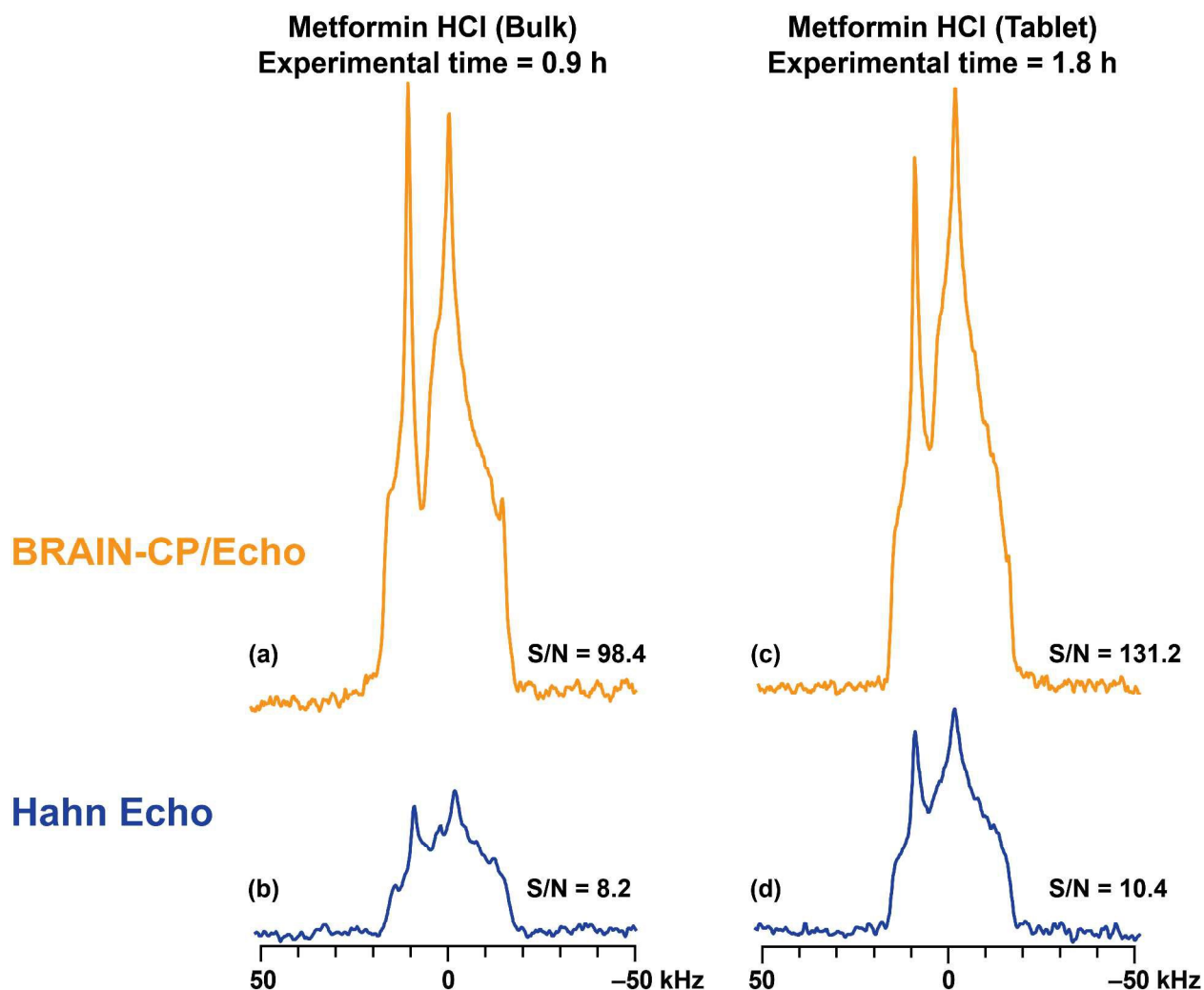


**Figure 2.** Comparison of DE and BCP acquisition methods at 9.4 T. For the bulk sample of **Metf**,  $^{35}\text{Cl}$  SSNMR spectra were acquired in the same length of time (0.9 h) using (a) the BRAIN-CP/Echo pulse sequence (CP) and, (b) the Hahn-echo pulse sequence (DE). For the dosage form, spectra were acquired in 1.8 h using (c) the BRAIN-CP/Echo pulse sequence, and (d) the Hahn-echo pulse sequence.

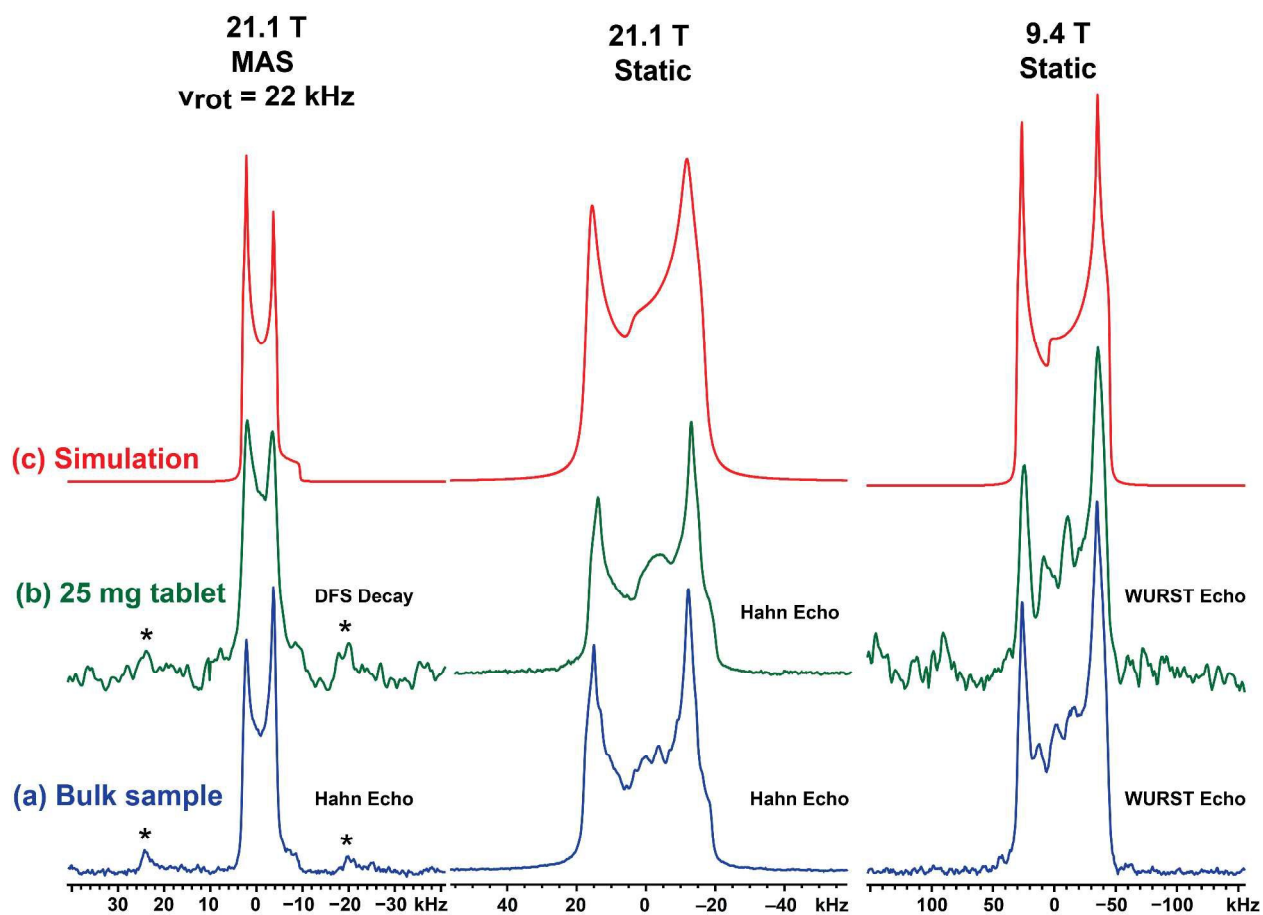


**Figure 3.**  $^{35}\text{Cl}$  SSNMR spectra of the (a) bulk **Diph** sample, (b) **Diph** dosage form, and (c) analytical simulations. Spinning sidebands are denoted by \*.

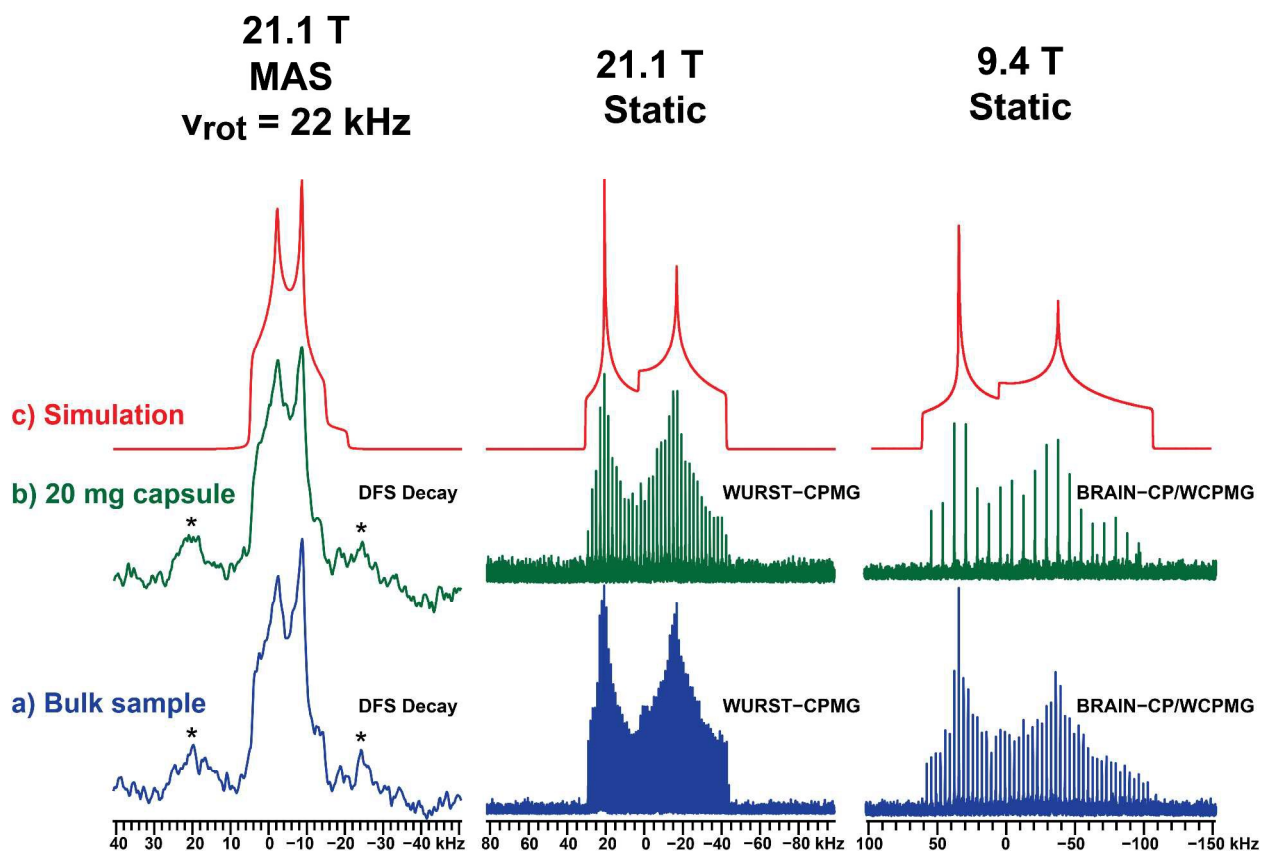


**Figure 4.**  $^{35}\text{Cl}$  SSNMR spectra of the (a) bulk **Nica** sample, (b) **Nica** dosage form, and (c) analytical simulations. Spinning sidebands are denoted by \*. The resolution of the spectra of the capsule (at 9.4 and 21.1 T) is of lower resolution than those of the bulk. The spikelet separation was increased for the dosage form in order to maximize S/N (see the **Supporting Information** for acquisition parameters).

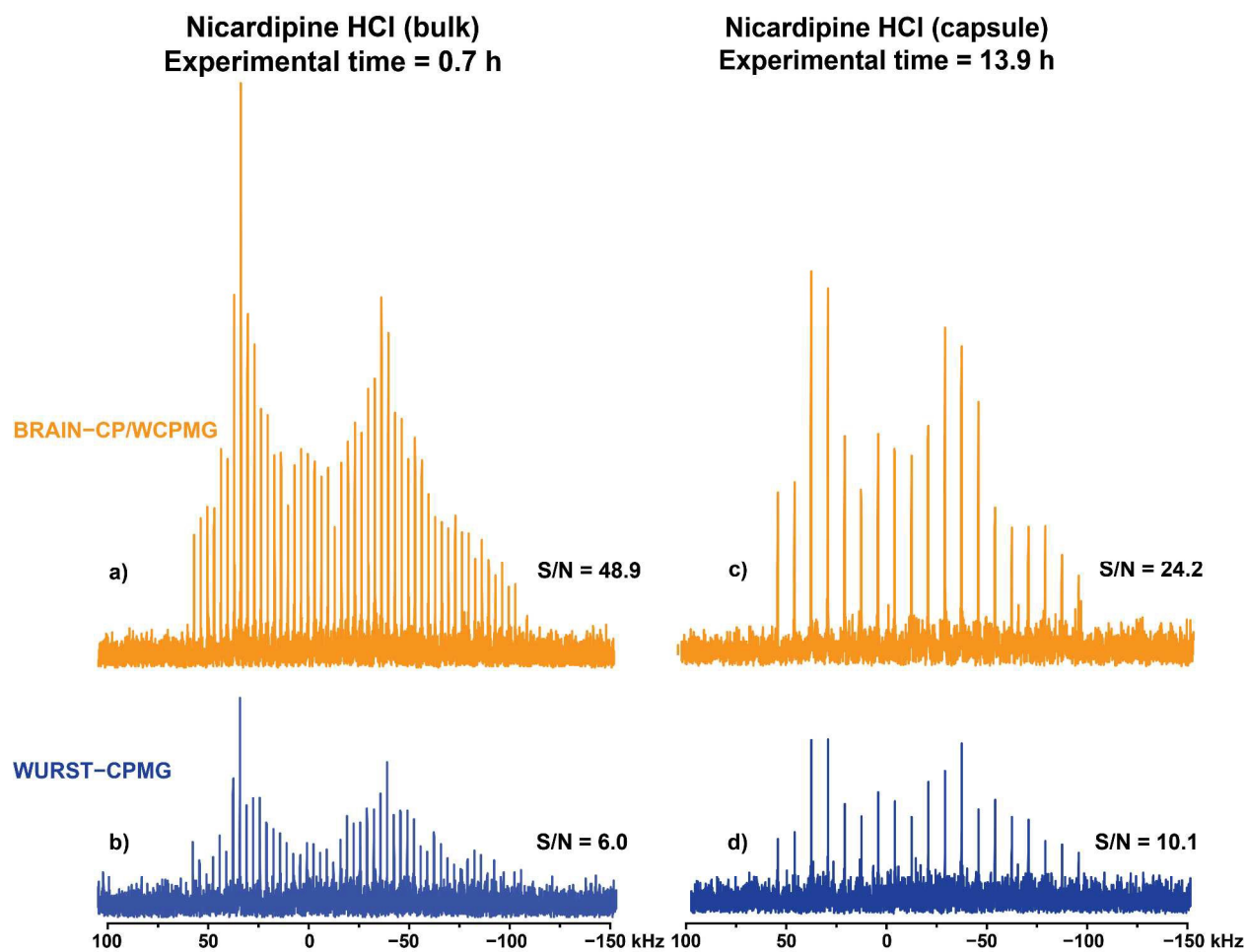


**Figure 5.** Comparison of DE and CP acquisition methods at 9.4 T. For the bulk sample of **Nica**,  $^{35}\text{Cl}$  SSNMR spectra were acquired in the same length of time (0.7 h) using (a) the BRAIN-CP/WQCPMG pulse sequence (BCP) and, (b) the WURST-QCPMG pulse sequence (DE). For the dosage form, spectra were acquired in 13.9 h using the same (c) BCP and (d) DE methods.

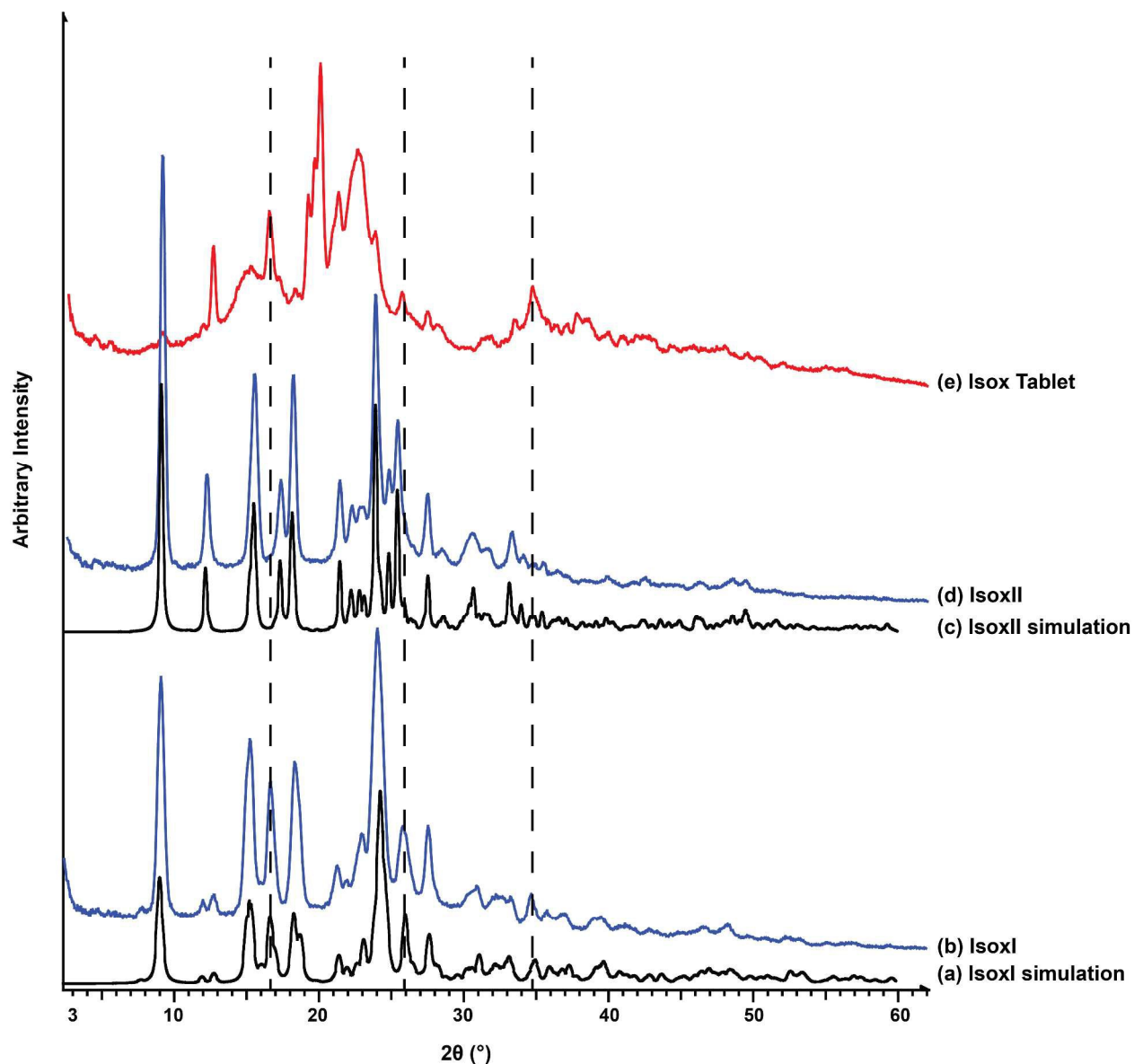


**Figure 6.** The (a) simulated pattern of the structure of **Isox-I**,<sup>50</sup> (b) experimental pXRD pattern of **Isox-I**, (c) simulated pattern of the structure of **Isox-II**,<sup>83</sup> (d) experimental pXRD pattern of **Isox-II**, and (e) experimental pXRD pattern of the **Isox** tablet. Peaks that are common between the **Isox** tablet and Isox-I are indicated by dashed lines.

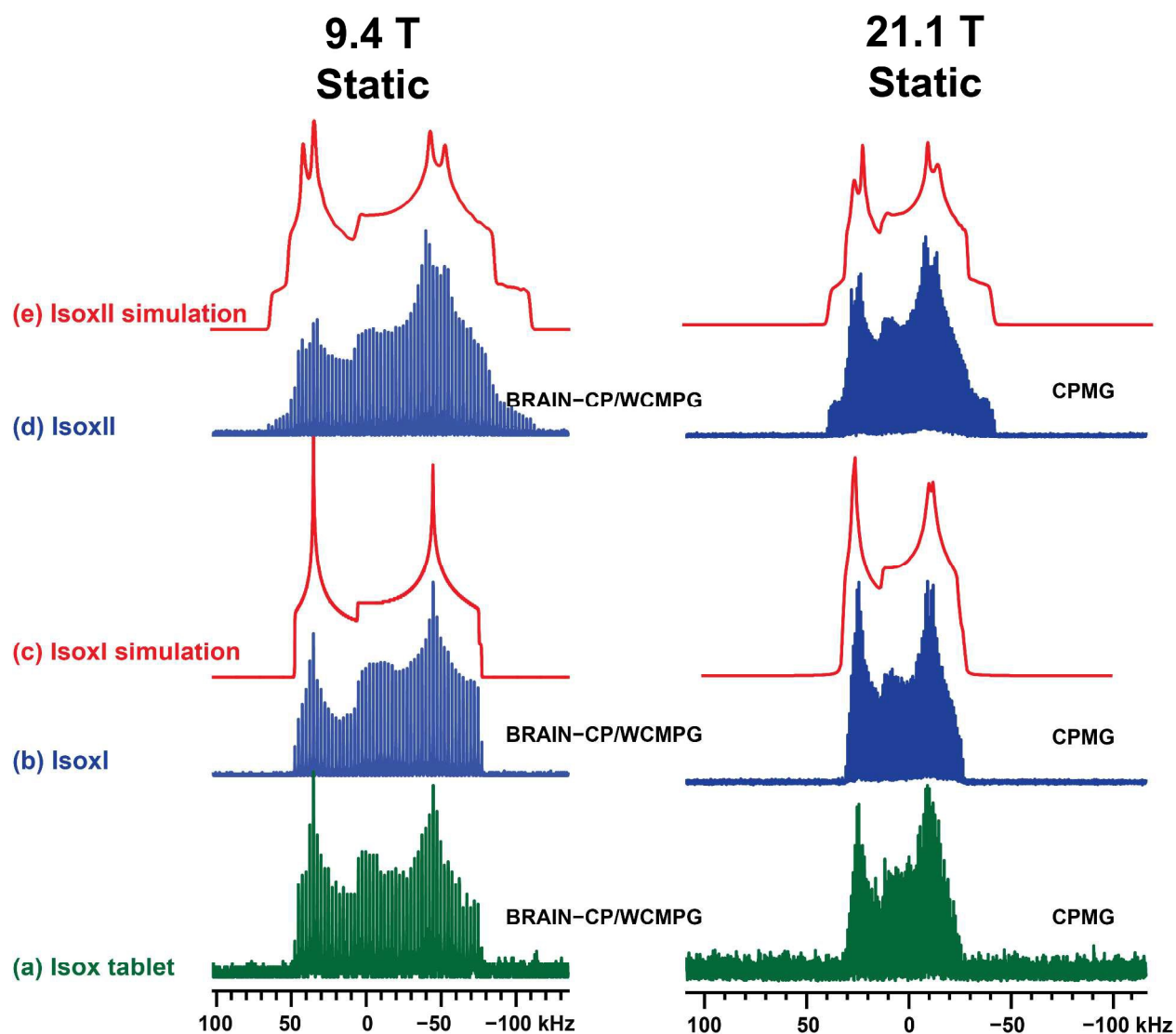


**Figure 7.** Static  $^{35}\text{Cl}$  SSNMR spectra of Isox polymorphs: (a) Isox dosage form, (b) Isox-I, and (d) Isox-II. The corresponding analytical simulations for (c) Isox-I and (e) Isox-II.

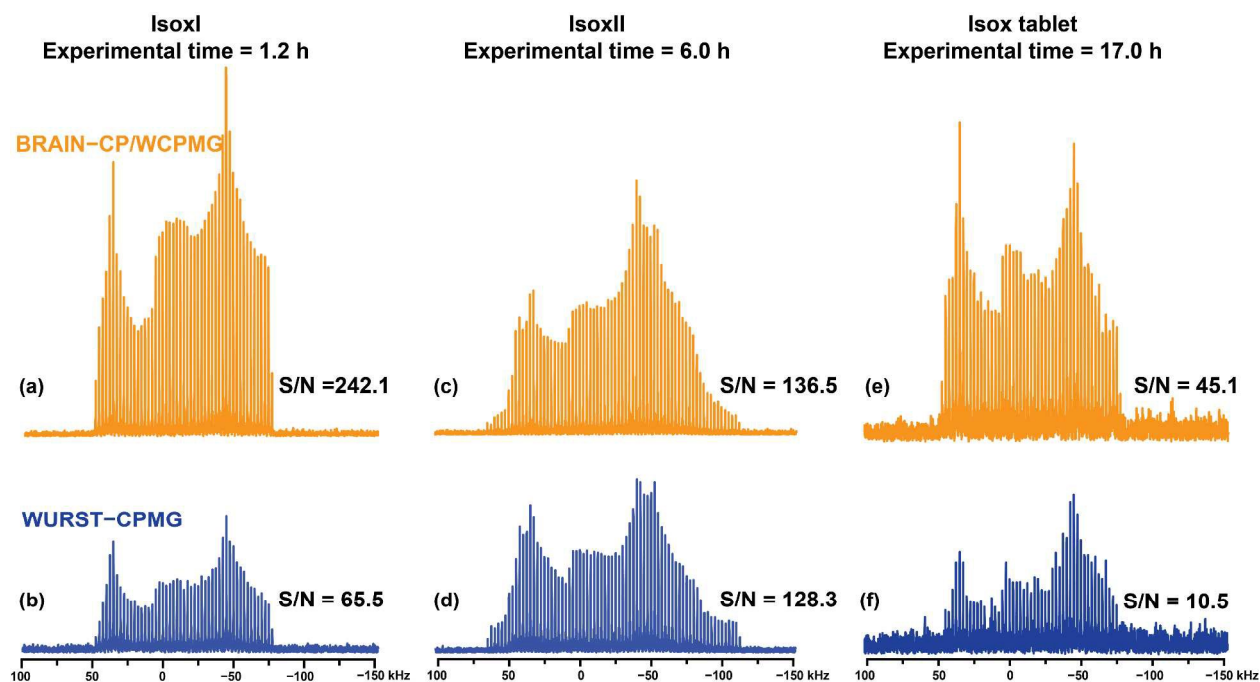


**Figure 8.** Comparison of DE and BCP acquisition methods at 9.4 T. For **Isox-I**,  $^{35}\text{Cl}$  SSNMR spectra were acquired in the same length of time (1.2 h) using (a) the BRAIN-CP/WCPMG pulse sequence (BCP) and (b) WURST-CPMG pulse sequence (DE). For **Isox-II**, spectra were acquired in 6.0 h using (c) BCP and (d) DE. For the **Isox tablet**, spectra were acquired in 17.0 h using (e) BCP and (f) DE.

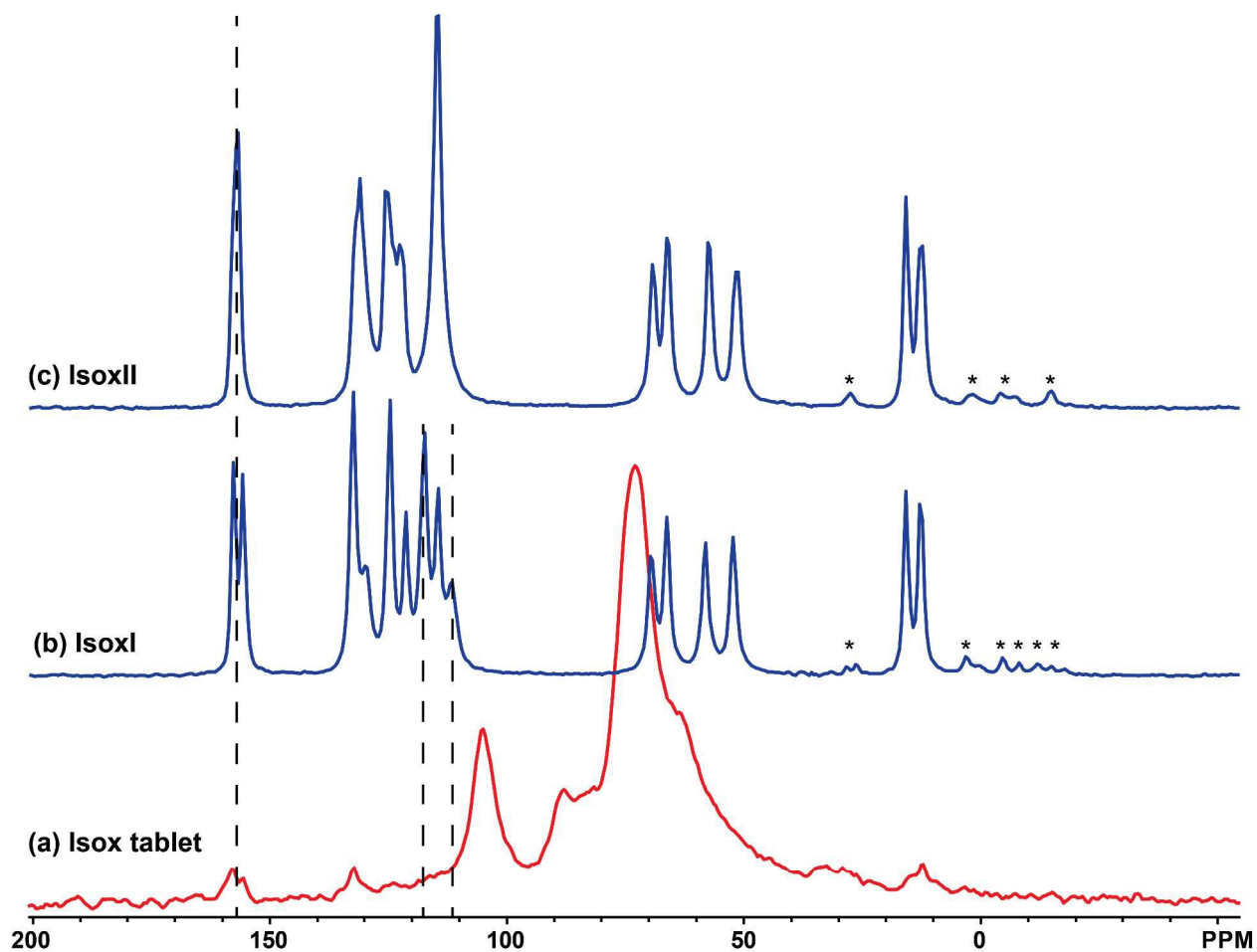


**Figure 9.**  $^1\text{H}$ - $^{13}\text{C}$  VACP/MAS (9.4 T) SSNMR spectra of (a) the **Isox** tablet, (b) **Isox-I**, and (c) **Isox-II** acquired with  $\nu_{\text{rot}} = 13$  kHz. Spinning sidebands are denoted by \*. Dashed lines indicate  $^{13}\text{C}$  chemical shift fingerprint regions.

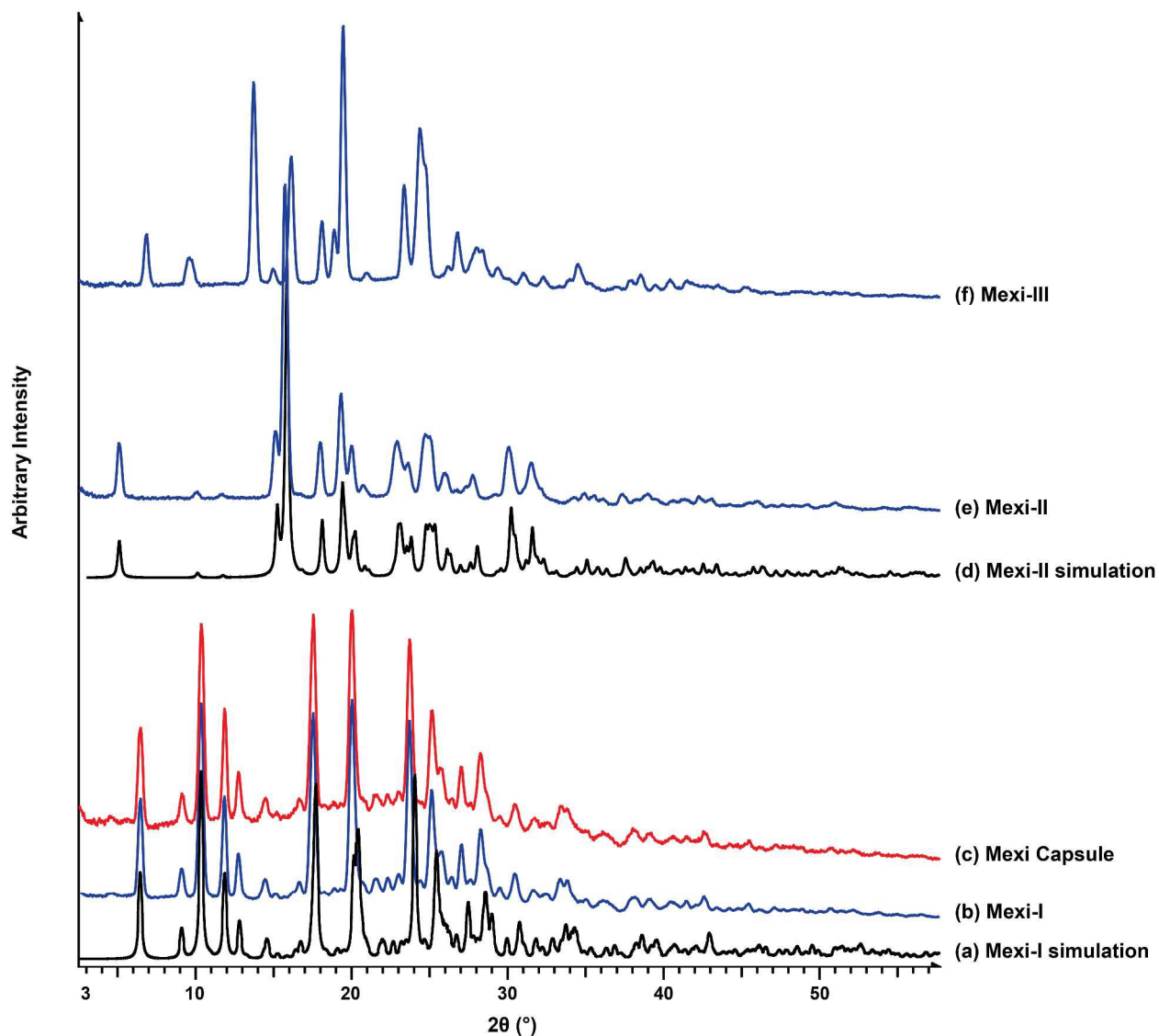


**Figure 10.** The (a) simulated pattern of the reported crystal structure of **Mexi-I**,<sup>51</sup> (b) experimental pXRD pattern of **Mexi-I**, (c) experimental pXRD pattern of the **Mexi** capsule, (d) simulated pattern of the single crystal structure of **Mexi-II**, (e) experimental pXRD pattern of **Mexi-II**, and (f) experimental pXRD pattern of **Mexi-III**.

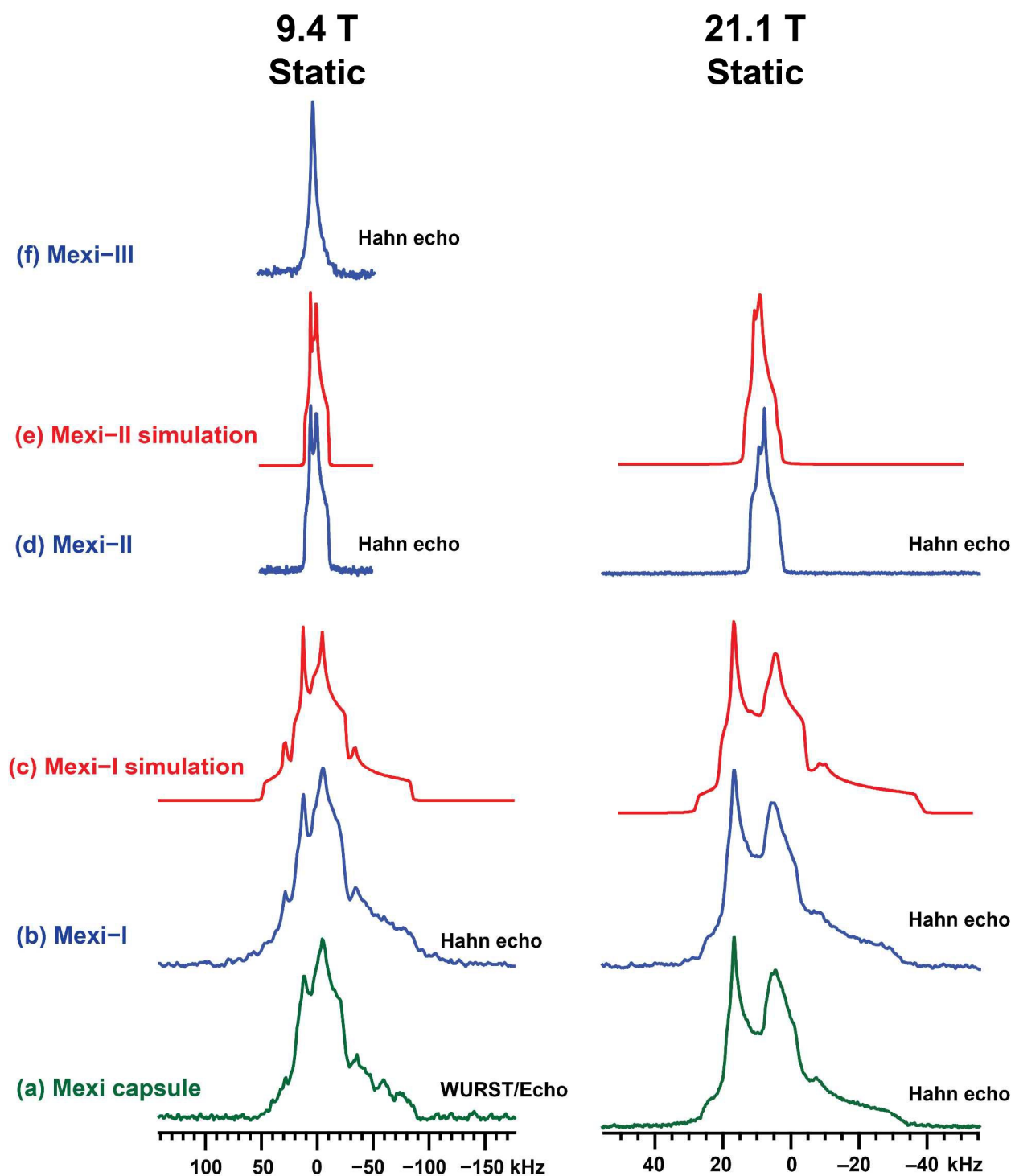


**Figure 11.** Static  $^{35}\text{Cl}$  SSNMR spectra of Mexi polymorphs: (a) Mexi dosage form, (b) Mexi-I, (d) Mexi-II, and (f) Mexi-III. The corresponding analytical simulations of (c) Mexi-I and (e) Mexi-II are shown in red. Simulation of the Mexi-III spectrum was not possible due to the lack of spectral features.

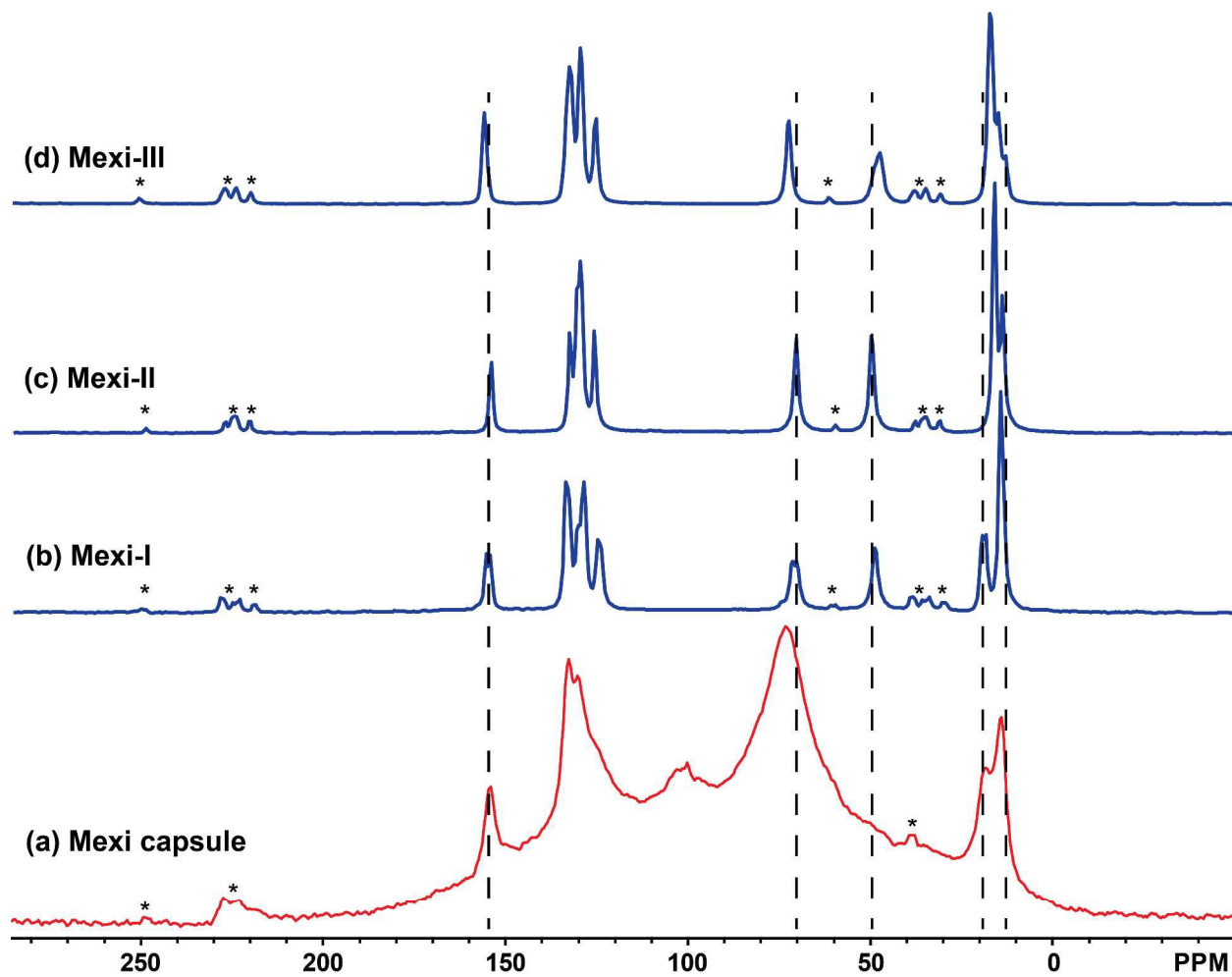


**Figure 12.**  $^1\text{H}$ - $^{13}\text{C}$  VACP/MAS (9.4 T) SSNMR spectra of (a) the **Mexi** dosage form, (b) **Mexi-I**, (c) **Mexi-II**, and (d) **Mexi-III** at  $\nu_{\text{rot}} = 9.5$  kHz. Spinning sidebands are denoted by \*. Dashed lines indicate  $^{13}\text{C}$  chemical shift fingerprint regions.

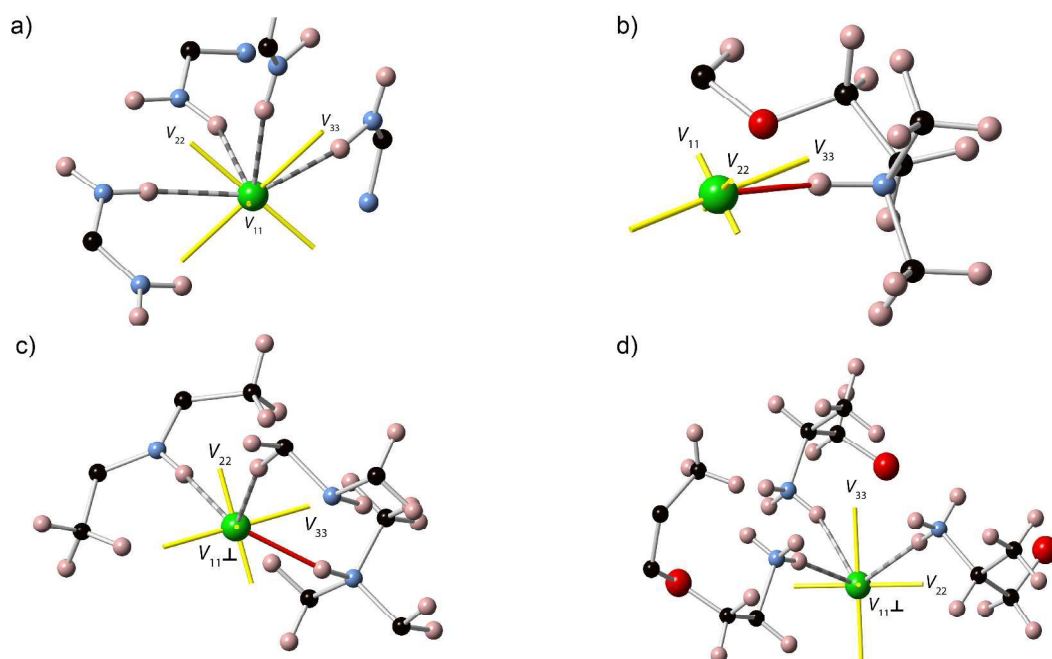


**Figure 13.**  $^{35}\text{Cl}$  EFG tensor orientations for the fully optimized structures of: (a) **Metf**; (b) **Diph**; (c) **Nica( $\beta$ )**; and (d) **Mexi-II**. Contacts that are shorter than 2.1 Å and shorter than 2.6 Å are illustrated with solid red and dashed grey lines, respectively. In each of the diagrams of the Cl environments, only H atoms involved in  $\text{H}\cdots\text{Cl}$  contacts that are less than 2.6 Å are displayed (H atoms involved in hydrogen-bonding to Cl anions are always covalently bound to either N or O).